Shear-Zone Hosted Gold and Silver Deposits in the Sierra Cacachilas,

Baja California Sur, Mexico

by

Allison Rose Severson

A Thesis Presented in Partial Fulfillment
of the Requirements for the Degree
Master of Science

Approved July 2015 by the
Graduate Supervisory Committee:

Stephen J. Reynolds, Chair
Steven Semken
Donald Burt

ARIZONA STATE UNIVERSITY
August 2015

ABSTRACT

The historic Cacachilas mining district is located in Baja California Sur, approximately 20 kilometers east of La Paz, and has a series of gold- and silver-hosted veins, faults, and shear zones within Cretaceous granodioritic plutons. The remote geographic location and past political events within Mexico left the district essentially unexplored after the late 1800s, when the Mexican Revolution began. More recent discovery of gold deposits along the Baja peninsula instigated a renewed interest in mineralization in the Sierra Cacachilas. The area lacks detailed previous geologic data, so this study focused on characterizing the controls of mineralization and the locations of mineralized trends of deposits within the northeastern Sierra Cacachilas, with a goal toward helping assess economic viability of the deposits. I mapped surficial geologic data, such as outcrop locations, alteration assemblages, limonite intensities, and structural measurements. I then synthesized these into geologic maps and cross sections. I combined field data with geochemical assays and structural plots to better characterize individual historic district trends and newly located trends to understand the distribution of mineralization at surface and at depth. Lastly, I synthesized geology of the Sierra Cacachilas with other gold and silver deposits located in the southern Baja peninsula to better characterize the mineralization and deposit style of the Cacachilas district.

Mineralization in the northeastern Sierra Cacachilas is mainly restricted to steeply dipping quartz veins, faults, and brittle-ductile shear zones that trend generally northeast. Some veins are en-echelon within the mineralized zones, implying some lateral movement along the zones. Veins are dominated by milky to clear quartz with trace sulfides, abundant

limonite (after sulfides), and local open-space textures. Mineralization is interpreted to be intermediate between classic epithermal and mesothermal veins. Within mineralized trends and commonly associated with mineralization are greisen-like zones that are defined by intense sericitic to muscovitic overprint, trend northeast, and are with or without sulfides. The intensity of sulfide abundance and limonitic alteration after sulfides within and near mineralized zones is overall a good guide to mineralization. Based on past reports and on my recent studies, the Cacachilas district has very promising potential for relatively small, high-grade deposits.

AKNOWLEDGEMENTS

I want to thank my family and friends for your continued love and support. My parents, for passing on their geologic knowledge and sharing many a conversation with me about geology and life. My friends, for our many intellectual discussions.

Thank you to the entire Reynolds family for all of your logistical, logical, and emotional support; Dr. Stephen Reynolds for sharing your exhaustive structural and Arizona geology knowledge. Cowboy, Fran, Zak, Stoney, and Shane for all of your unwavering support and fun times in the Baja.

Thank you to my original geology posse at the University of Minnesota Duluth who made the subject so amazing, and got me hooked. Your hard work, determination, support, and love for your work is inspiring. Thank you for sharing your passion with me.

Last, but certainly not least, a sincere thank you to my fellow Wasatch Uinta Field Camp instructors for the most amazing action-, knowledge-, and stress-filled summers a girl could hope for and for all of the opportunities we've made together. I wouldn't have made it this far if it weren't for my home away from home. I find it a true blessing to have such intelligent, humble, and helpful folks in my life. Cheers to what comes next!

TABLE OF CONTENTS

CHAPTER Page

CHAPTER Page

LIST OF TABLES

LIST OF FIGURES

Figure Page

Figure Page

Figure Page

1. INTRODUCTION

1.1 LOCATION

The Sierra Cacachilas, located along the N24.10^{o} latitude, are approximately 25 kilometers east of city of La Paz, Baja California Sur, Mexico and 8 km northwest of the town of El Sargento (Figure 1.1). This mountain range is host to the historic Cacachilas mining district, which at a regional scale is located on the northernmost edge of the Los Cabos Block (LCB) (Figure 1.2). The LCB is a pluton-dominated terrane separated from the rest of the Baja by a series of north-trending shear zones and faults that juxtapose eastern batholithic rocks against western volcanic rocks. The Sierra Cacachilas provide insight on the geologic and tectonic history of the Baja California, and more importantly, the numerous small-scale Au-Ag deposits that are located along the southern end of Baja California Sur.

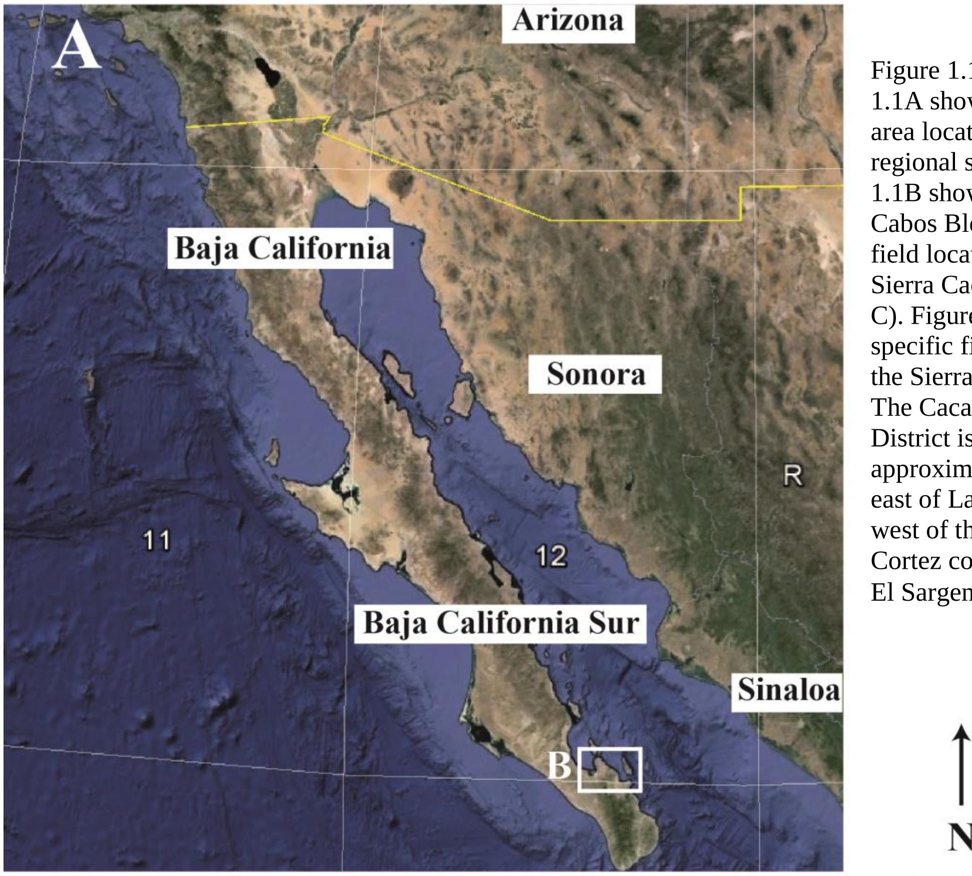

Figure 1.1 (A-C). Figure 1.1A shows the field area location (B) at a regional scale. Figure 1.1B shows the Los Cabos Block area and field location in the Sierra Cacachilas (Box C). Figure 1.1C outlines specific field area within the Sierra Cacachilas. The Cacachilas mining District is located approximately 25 km east of La Paz and 8 km west of the Sea of Cortez coastal town of El Sargento.

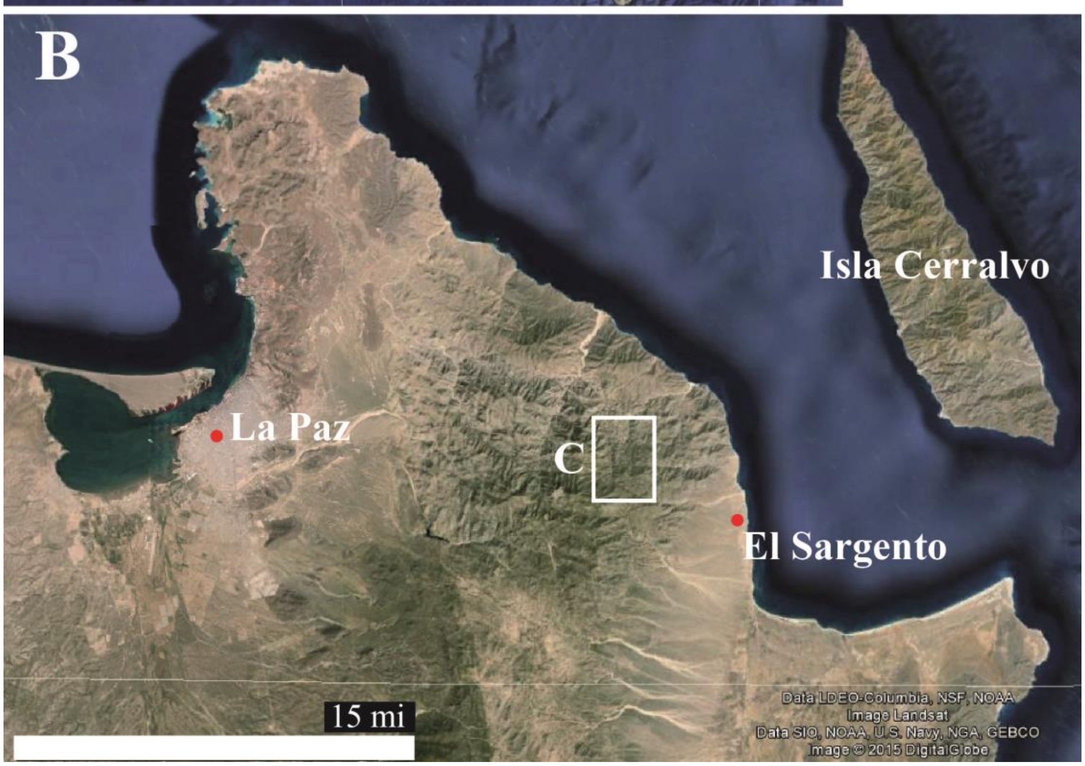

1.2 PURPOSE OF STUDY

The historic Cacachilas mining district remains vastly underexplored since the early 18^{th} century and provides a unique opportunity for green-field exploration of Au-Ag-hosted mineralized shear zones located throughout the district and the peninsular region. Extensive geophysical data have been collected, but relatively little surficial geologic analysis of the rocks has been done to-date. In this study, a compilation of geologic, structural, and limonite alteration data are used to better understand the surface geology. Historic trends within the district are used to better constrain known mineralization. I use exploration mapping of unexplored areas to find potential trends within the northeastern sector of the Cacachilas district. Field data, geologic maps, and assay results from the Cacachilas district constrain the deposit style, while a synthesis of known nearby deposits on the southern tip of the Baja (Figure 1.2) help to understand the Cacachilas district at a regional scale.

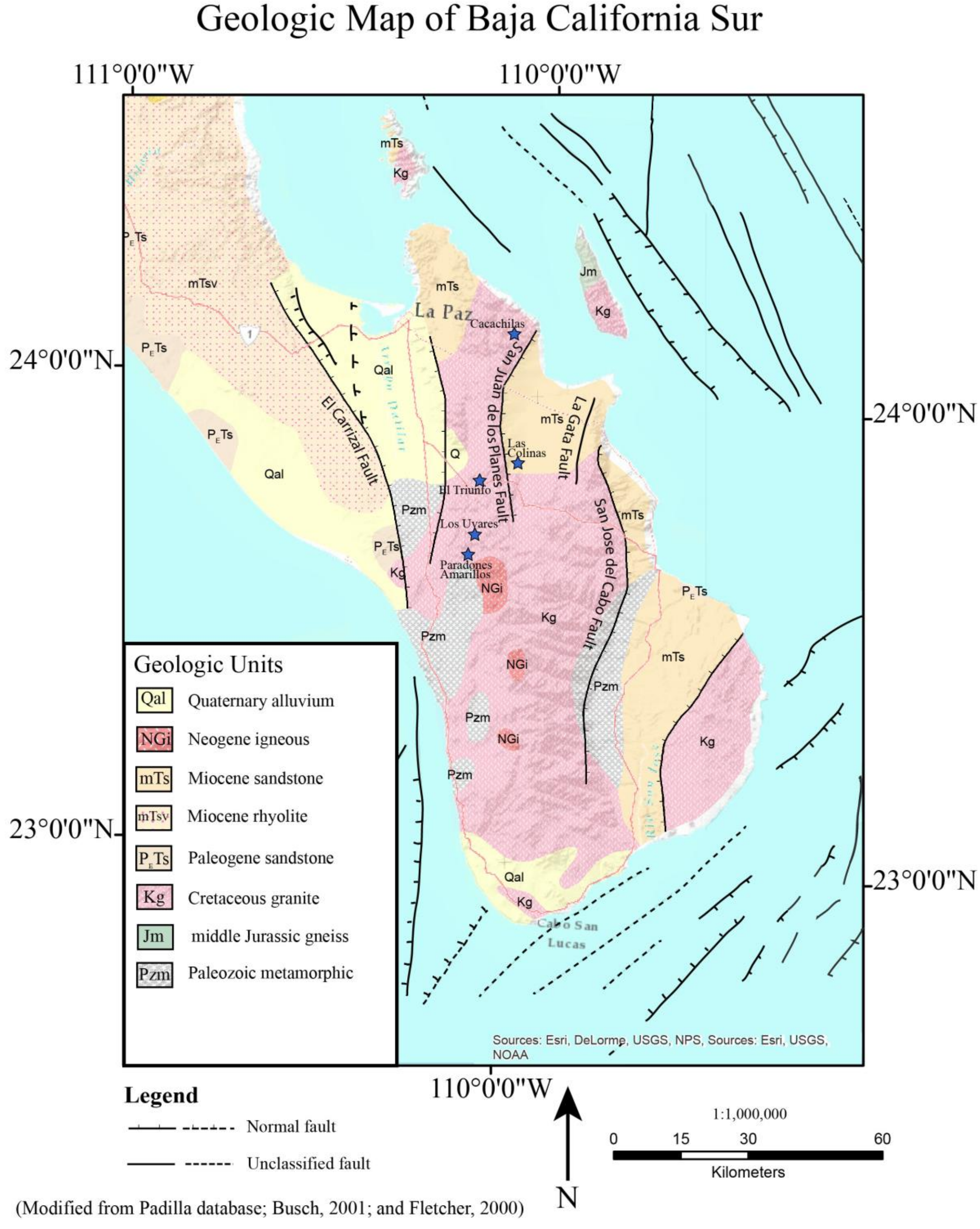

Figure 1.2. Geologic map of the southern tip of the Baja California Sur. The El Carrizal Fault and the La Paz Fault (labeled in figure) are examples of shear and fault zones that geologically separate the LCB terrane from the rest of the Baja California. Dominantly volcanic rocks lie west of the fault zone, whereas dominantly igneous and mafic rocks lie east of the zone. Similar deposits to the Cacachilas are labeled and marked by stars.

2. BACKGROUND

2.1 REGIONAL GEOLOGIC HISTORY OF BAJA CALIFORNIA SUR

Several accreted terranes make up the Baja California Peninsula. Our study focuses on the Los Cabos Block (LCB), which occupies the southern tip of the peninsula from La Paz to Cabo San Lucas (Figure 1.2). The LCB is separated from the rest of the peninsula by a fault zone that runs through La Paz; this zone is referred to as the La Paz Fault Zone (LPFZ). One interpretation of the LPFZ is a suture plane between the LCB and rest of the peninsula (Figure 1.2) (Hausback, 1984; Schaaf et al., 2000). The LPFZ is mostly covered by Quaternary units; therefore, sense of motion along the fault is poorly constrained and poorly understood. Instead, exposure of Mesozoic rocks closest to the boundary are used to infer the contact between the LCB and the rest of the peninsula (Sedlock, 2003). Where exposed, the LPFZ has been classified by researchers as either normal or right-lateral strike-slip, or a combination of the two (Hausback, 1984). However, other researchers have proposed that the LPFZ is not a fault, but a buttress unconformity separating younger and older units (Fletcher and Munguia, 2000). The geology of the southern peninsular region is dominantly Cretaceous plutons, part of the Peninsular Ranges batholith. The Sierra Cacachilas are located on the LCB and are composed of almost entirely plutonic rocks that are approximately 92.5 Ma (Wachtor, unpublished). Remnants of prebatholith geology are preserved as roof pendants between individual plutons; these pendants provide important clues to the geologic history before the extensive period of intrusive igneous activity. The batholiths host older roof pendants and are overlain by Cenozoic sedimentary and volcanic units.

2.1.1 Pre-batholith History

Pre-batholithic history of Baja California is not well documented and understood. Little is known about the geologic history of Baja California before Cretaceous plutonism dominated the coast. However, remnants of Paleozoic metasedimentary rocks and Triassic to Jurassic metasedimentary and metavolcanic rocks, known as roof pendants, survived Mesozoic plutonism in some parts of Baja California. These roof pendants are significant in piecing together the pre-batholith history. Paleozoic metasedimentary rocks in Baja California were likely formed in a passive continental margin, temporally similar to the northern Cordilleran continental margin. Triassic-Jurassic metavolcanic units represent a continental margin arc, contemporaneous to the arc along western North America.

The Baja peninsula is part of the Guerrero superterrane that extends along a northeast trend into central Mexico. The Guerrero superterrane is composed of Mesozoic volcanogenic crust associated with a proposed intra-oceanic island-arc system (Dickenson, 2001). The associated Alisitos arc, located along western Baja California, is also a part of the Guerrero superterrane and is interpreted to have been separated from North America by an ocean basin during the Cretaceous (Busby et al., 1998; Alsleben, 2012). The oceanic basin eventually collapsed under a compressional regime that resulted in subduction-related plutonism, a suture zone, and a fold-thrust belt. These features represent the accretion of the Alisitos arc and Guerrero superterrane onto mainland Mexico via late Early Cretaceous arc-continent collision (Alsleben, 2012; Dickenson, 2001). As Cretaceous arc-continent collision and subduction initiated, resultant pluton emplacement metamorphosed volcanic and sedimentary roof pendants up to amphibolite facies and began forming the Peninsular Ranges Batholith (Fletcher et al, 2000; Alsleben, 2012).

2.1.2 Mesozoic History – Batholith Emplacement

The beginning of the Mesozoic is signified by the break-up of the supercontinent, Pangaea. This directional change of plate motion initiated eastward movement of the Farallon plate towards a westward-moving North America. Continental arc collision, such as during the Sonoma Orogeny, was the subsequent main tectonic process, and subduction and island-arc to continental-margin volcanism ensued shortly thereafter. The Baja California peninsula was still attached to mainland Mexico throughout the Cretaceous and most of the Cenozoic.

Subduction-related magmatism occurred along the western edge of North America circa 140-90 Ma (Schaaf, 2000; Busby, 2004). The Peninsular Ranges Batholith (PRB) runs along the entire length of the Baja and is a series of deformed and undeformed continental margin-related tonalitic to granitic intrusions. The contact between the mafic Western Peninsular Range Batholith (WPRB) and the felsic Eastern Peninsular Range Batholith (EPRB) may represent closure of the proposed aforementioned oceanic basin (Busby, 2004).

The LCB is separated from the rest of the Baja California Sur by the La Paz fault zone, which acts as a suture between terranes. Composed mostly of subduction-related rocks, the LCB represents a west-rotated block of a magmatic arc, ranging west to east from gabbro to granodiorite and peraluminous granite, to roof-pendant pre-batholithic metasedimentary rocks, respectively (Fletcher et al, 2000). The LCB is largely regarded as an isolated exposure of the Cretaceous batholith of western North America Cordillera. Scientific literature debates the provenance of the Los Cabos Block in southern Baja; while some believe the block can be traced back to a similar felsic batholith in Puerto Vallarta, mainland Mexico (Shaaf, 2000; Hausback, 1984), new geological and geophysical data have recently suggested that the LCB is instead a part of the Peninsular Range Batholith (PRB) of central to northern Baja (Kimbrough 2014). Furthermore, the transgression from west to east of gabbroic rocks to granitic plutonism along the Los Cabos block appears to reflect similarities to the WPRB and EPRB that trend along the long axis of the Baja.

2.1.3 Post-Batholith (Cenozoic) History

Subduction continued through the Cenozoic, resulting in eastward migration of calc-alkaline volcanism and exhumation of Mesozoic plutons (Hausback, 1984; Schaaf, 2000). Slab shallowing may have pushed mantle wedge flow further inland explaining the eastward transgression of volcanism. The complete subduction of the Farallon plate beneath North America occurred approximately 25-12 Ma (Hausback, 1984), and resulted in the Pacific plate pushing into North America at an oblique angle. This collision resulted in temporary subduction of the Pacific-Farallon spreading ridge beneath North America before spreading center-induced stress was accommodated along the plate boundary by conversion to transpressional motion. This transpressional motion is a synthetic San Andreas system and governs tectonism from the Cenozoic to the present.

Development of the Mendocino triple junction near southern California and the Rivera triple junction near northern Baja California further enforced transpressional motion (Stock and Hodges, 1989; Fletcher and Munguia, 2000); the Mendocino triple junction migrated northward, and the Rivera triple junction continued southward (Figure 2). Micro-plates formed along Baja California at approximately 20-12 Ma and were eventually captured by the Pacific plate. The Baja California microplate was completely separated from North America ca. 3.5 Ma and gradually transferred to the Pacific plate (Hausback, 1984; Stock & Hodges, 1989), but GPS plate motion studies suggest that transfer is ongoing (Dixon et al, 2000). While Baja California is moving in the same direction as the Pacific plate, it is doing so at a slower rate (Dixon et al, 2000). The partial coupling between Baja and the Pacific plate may be due to shearing of the microplate on the Pacific plate along a zone of pre-existing weakness, similar to that observed in the San Andreas system (Plattner et al., 2007). Evidence of microplate capture is inferred by the Tosco-Abreojos fault, to the west of the Baja California (Figure 2), which developed from a trench to a dextral strike-slip fault zone before the plate boundary migrated or jumped east into the Sea of Cortez and Gulf Extensional Province (Stock and Hodges, 1989; Fletcher and Munguia, 2000; Busch et al, 2011).

During the Miocene, rifting began between mainland Mexico and what is now Baja California Sur (Stock and Hodges, 1989; Atwater, 1970). Sea-floor spreading was fully onset circa 3.6 Ma (Fletcher et al., 2000) and formed the present-day Sea of Cortez, or Gulf of California. Opening of the Gulf created faults along Baja, likely tilting the peninsula westward. Spreading centers within the Gulf are narrow, and are defined by an axial array of en echelon, oblique transform faults (Figure 2) (Fletcher et al., 2000). Miocene calc-alkaline volcanism formed volcanic strata that have since been tilted. The La Paz fault runs through Mesozoic plutons and Miocene volcanics, limiting deposition of the volcanics to the east. As relative normal and strike-slip motion along the fault created a west-facing buttress, stopping transport of material (Hausback, 1984; Fletcher et al., 2000).

The Gulf of California represents an oblique-divergent rift with transform faults and spreading centers along the main zone of deformation along the plate boundary between the North America and Pacific plates (Figure 2). Associated with the main zone of rifting are left-stepping normal faults that strike obliquely and form on the margin (Busch et al., 2011; Withjack and Jamison, 1986). The Gulf axis is represented by long dextral strike-slip faults and is separated by shorter spreading centers. The southernmost portion of Baja California Sur, also known as the LCB, is geologically separated from the rest of the Baja by what is likely a set of north-striking, east-dipping normal faults with dextral slip (Figure 2) (Busch et al., 2011). These faults have been characterized as the gulf-margin system (Fletcher and Munguia, 2000), range Miocene to Pliocene in age, and represent the transitional stage from rift-to-drift with the initiation and continuation of continental rifting.

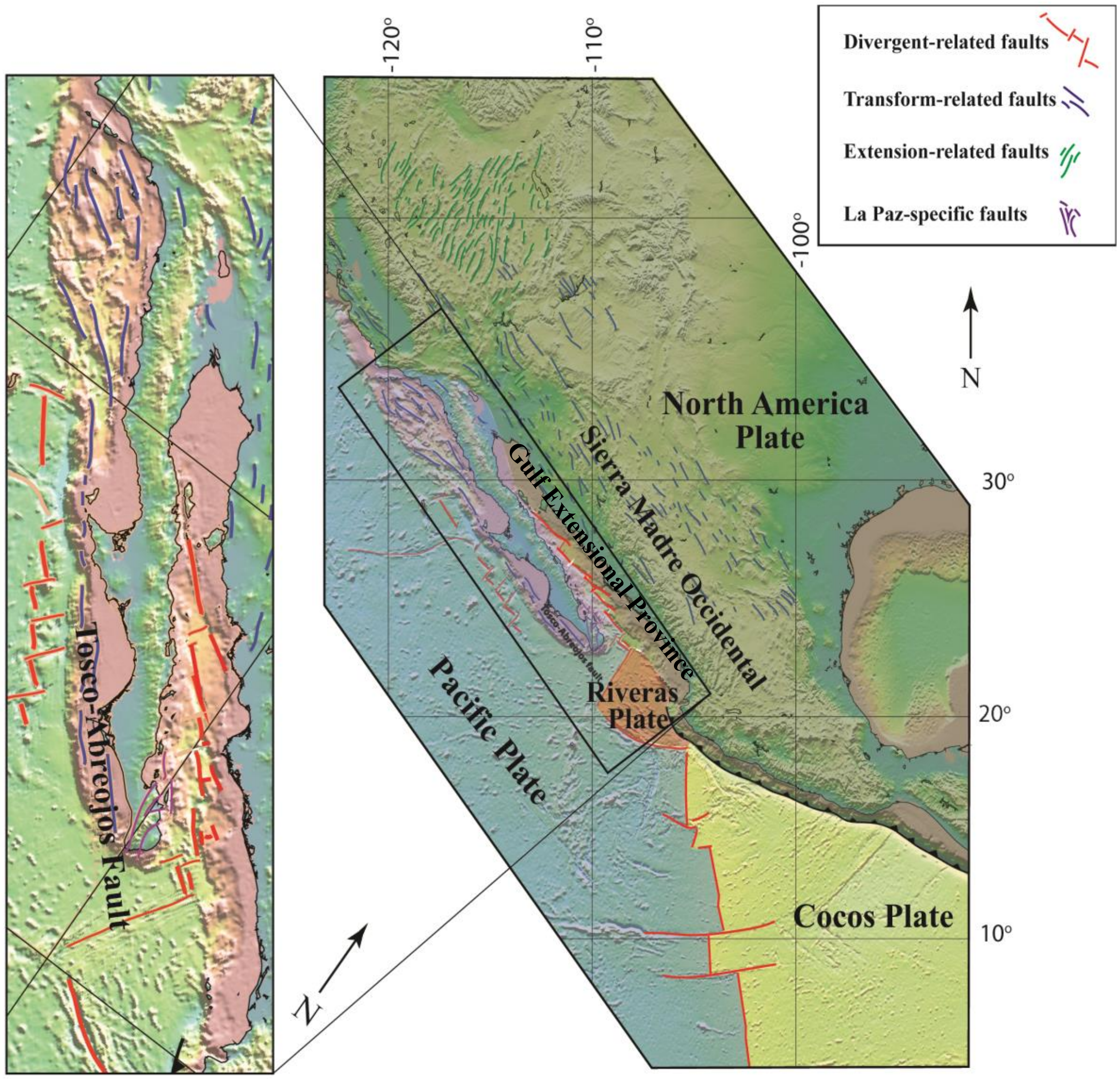

Figure 2.1. Present tectonic setting of current Mexico and the Gulf of California region. Modified from Scripps satellite geodesy global topography (Smith and Sandwell, 1997).

2.2 HISTORY OF GEOLOGIC EXPLORATION AND MINING

Mining of gold and silver throughout Baja California began in the 1700s, shortly after Jesuit missionaries colonized mainland Mexico and the Baja California in 1697 (Orynski, 1889). Eventually, the Jesuits were forced from the area, leaving little to no trace of their mining operations. It wasn't until the 1800s that mining began to prosper in Baja. Historic districts are located throughout the southern tip of the Baja, including ones near San Antonio, south of the field area. The historic towns of El Triunfo and San Antonio were developed to accommodate mine workers and families. Mining surrounding these towns has since essentially halted, but active mines and exploration sites are still interspersed throughout Baja California (Figure 1.2).

The Cacachilas district (herein also known as "the district") was discovered by a rancher in 1841, who noticed a piece of "chloride of silver" float that had rolled down the mountains (Orynski, 1889). Mining of gold and/or silver began the same year and grew to host more than 15 operating mines within the district, including; Peruana, Rosario, Trinidad, Santa Lucia, Tesoro, Matancitas, San Gregorio, Tesorito, Las Animas, San Cayetano, La Casualidad, Santa Teresa, Anima Sola, La Soledad, Babelema, and Jesus Maria, among others (Orynski, 1889). Poor extraction methods and seasonal flooding forced miners to stay near-surface, thus many of the trends remain untouched and intact at depth. Furthermore, silver generally was the only element being extracted from the host rock, thereby leaving large amounts of gold, copper, and lead ore rock behind in waste piles. Mined until the late 1800s, the Cacachilas district was abandoned indefinitely at the start of the Mexican Revolution in 1910. In a rush to join the Revolution, miners hastily left behind ore piles that were ready to be placed on burro carts and sent away for processing. These piles still sit outside historic shafts within the district, affected by natural leaching of the ore rock. Since abandonment of the Cacachilas district in 1910, small-scale operations have since attempted to re-explore the historic district, but lack of previous knowledge and data of the area prove difficult in initiating property development.

This study expands on another Masters students' research in the Cacachilas district to the south of my field area, where Samuel Wachtor (in progress) followed historic trends and collected extensive assay data along trends. My research focuses on mapping geology, alteration, and structural controls along historic and newly discovered prospects in the northernmost portion of the district, including the historic trends of La Casualidad, Santa Teresa, La Libertad, Las Animas, Pisos, El Tesoro, and Matancitas. The overall goal of the exploration project is to locate and determine which of these historic trends are currently economic and to locate new prospective sites within the district. If developed, this historic district will once again provide jobs, metals, and recreational park land to the local Mexican community.

3. METHODS

3.1 MAPPING METHODS

Field work was conducted for a total of 33 days. Exploration mapping was completed on 1:5,000 - 1:2,500 scale topographic base maps using the zone 12N World Geodetic System 1984 (WGS84) coordinate system. To supplement low-resolution topographic maps, a hand-held Global Position System (GPS) was used to record tracks and locations of outcrops and workings. Attitudes of planar and linear features were measured by azimuth and right-hand rule convention using a Sylva Ranger compass. Magnetic declination was accounted for at 9^{o} E.

Three main mapping methods were used to record geologic, limonitic, and structural aspects. Geologic maps record outcrop location and rock type as well as tracks taken between location stops. Limonitic alteration may correlate strongly to mineralization, thus limonite maps record intensity of limonitic alteration at each outcrop. Qualitative analysis of limonite intensity is noted in the field using a (0-4) scale where: 0 indicates none; 1 indicates weak; 2 indicates moderate; 3 indicates strong; and 4 indicates pervasive limonite intensity (Appendix A). Structural maps record strike and dip of quartz veins, mineralized zones, dikes, and faults; they also record trend of quartz veins, mineralized zones, greisen zones, dikes, and faults where these features are poorly exposed or inferred from trend in float. A compilation of digitized field maps is presented in Chapter 4, section 2, titled "Geologic Maps and Cross Sections."

3.2 ASSAY SAMPLE COLLECTION

Assay samples were collected in the field, filling one 6" x 12" cloth bag per sample. A total of 29 samples were collected for assay. Assay preparation required refinement of collected field samples, crushing the material from each individual sample into two equal partitions of variable crush size (<1mm to 5 cm). One half was kept for reference and sample control, while the other half was sent out for assay. Half-samples were sent to ALS

Chemex in Hermosillo, Sonora for preparation, and were then sent to Vancouver, British Columbia, Canada for fire assay. Assay element results include Au, Ag, Cu, Pb, and Zn among others (Appendix B). Assay results published in text and Appendix B are expressed in parts per million (PPM), unless stated otherwise. For proprietary reasons, Au and Ag quantitative results are categorized into qualitative results, increasing in grade from; none reported, low, moderate, high, to very high. The ranges in values assigned to these subdivisions are deliberately not reported here.

4. RESULTS

4.1 FIELD RESULTS

The Sierra Cacachilas are dominated by pre-92.5 Ma Cretaceous felsic plutons, mostly granodiorite to tonalite, which are locally cut by two types of granitic dikes. Muscovite-rich greisen-like podiform structures cross-cut plutons and dikes, and are in turn cut by shear zones and faults. There is a major post mineralization east-west right-lateral fault that cuts through the field area and offsets mineralized trends. Descriptions of units identified and mapped in the field are discussed below.

The dominant rock unit in the district is a series of plutons, ranging from a granodiorite to tonalite with relatively minor amounts of primary potassium feldspar. Granodiorite to tonalite is light-gray (salt and pepper texture) where fresh, tannish-brown on weathered surfaces, and easily erodible and it breaks apart into mm-scale grains. Translucent, white quartz crystals (45-55%) are anhedral and range from 2-4 mm with minor amounts of 8 mm crystals; milky white plagioclase crystals (30-40%) are subhedral and range from 1-3 mm; pinkish tan potassium feldspar crystals (5-15%) are subhedral to euhedral and approximately 2-8 mm in length with some locations having prismatic crystals that range 2-7 cm in length; dark brownish black biotite crystals (5%) are anhedral and range from 0.5-1 mm in width, not forming thick stacks.

Two varieties of aplitic to locally coarser dikes cut the pluton, commonly with trends of approximately 150° – 170°. These dikes are differentiated mainly by color; the more common dike is identifiable by its distinctive pinkish color, whereas the less common dike has a distinctive white-gray color. Both of these dikes have a similar composition and crystal size, but pink granite dikes have a marginally higher potassium feldspar abundance.

Figure 4.1. An example of heterogeneous zone within the pink granite dike.

Pink granite dikes form mostly dikelets (1-10 cm in width) and minor dikes (approximately 1 m in width), with one distinct location forming a gently dipping sheet (a sill). Orange pink on weathered faces and light pink with stringers of dark pink on fresh surfaces, pink granite dikes are composed of smoky white quartz crystals (45-55%) that range from 0.5-1 mm, and are anhedral to subhedral; translucent pink potassium feldspar crystals (25-35%) that range from 0.5-1 mm, and are anhedral; milky white plagioclase crystals (15-20%) that range from 0.5-3 mm, and are anhedral; and metallic blue-gray oxides (<1%, trace) that are approximately 0.5 mm in length, and are anhedral. Locally within pink granite dikes are heterogeneous zones of coarse quartz, plagioclase, and potassium feldspar crystals that range up to 3 cm in length and 2 cm in width (Figure 4.1); approaching pegmatite in grain size.

White granite dikes form mostly dikelets (2-5 cm in width), and minor dikes (approximately 1-2 m in width). Grungy gray on weathered surfaces, and cream-colored on fresh surfaces, white granite dikes are composed of translucent light gray quartz crystals (45-55%) that range from 0.5-1 mm, and are anhedral; translucent gray pink potassium feldspar crystals (10-20%) that are 1 mm in length, and are anhedral to subhedral; and milky white plagioclase crystals (35-45%) that range from 0.5-1 mm, and are anhedral to subhedral.

Greisen-like pods cross-cut pluton and dikes and are distinguishable in the field by intense muscovite/sericitic alteration. Breakdown of biotite and primary potassium feldspar is commonly associated with alteration to sericite, secondary potassium feldspar, and minor amounts of kaolinite. Limonite alteration is commonly moderate to pervasive. Sulfides and metals form within pervasive box-work texture.

Quartz veins are the youngest unit to cut across the plutons, dikes, and greisen-like pods (Figure 4.2). Veins width range in thickness from sub-centimeter to several meters (Figure 4.3), and form an anastomosing pinch-and-swell pattern along trend. Veins vary along trend in sulfide abundance, texture, and amount of sericitic and potassic alteration (Figure 4.3), where potassic alteration refers to the introduction of secondary potassium feldspar. Texture of quartz veins ranges from translucent prismatic quartz crystals with strong to pervasive limonite alteration and trace sulfide abundance (Figure 4.3C) to milky white quartz veins with no to weak limonite alteration and minor amounts of sulfides

Figure 4.2. Cross-cutting relationship depicting a 1-2 cm in width quartz vein running through granodiorite pluton and pink granite dike; quartz vein is outlined in red dashed lines.

(Figure 4.3A & 4.3B). Milky white quartz veins are further distinguished in character by milky white veins with sulfides peppered along the edges (Figure 4.3A & 4.3B) and by milky white quartz veins with brecciated clasts and no visible sulfides (Figure 4.3D).

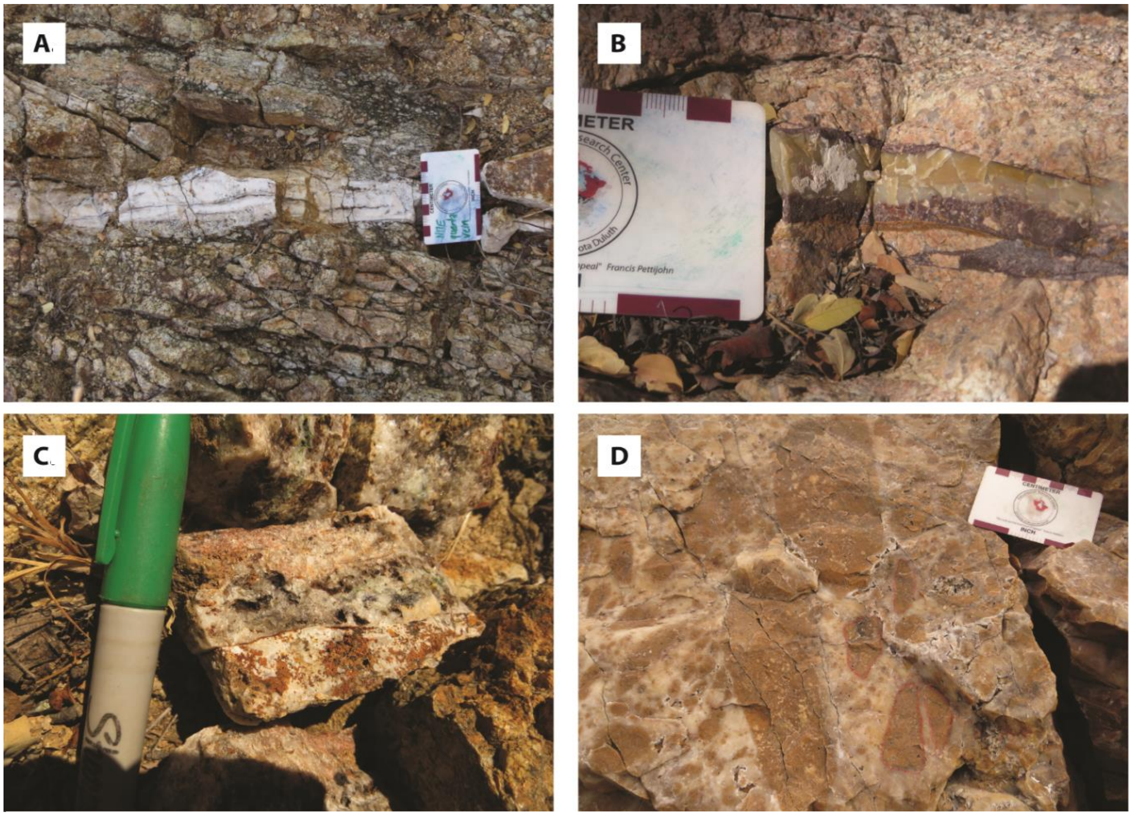

Figure 4.3. Quartz vein variability in width and composition. Quartz veins range in size from approximately 2 cm (B) to 50 cm (D) and range in quartz variety from milky white and crystalline (A), orange-brown and peppered with sulfides (B), pervasive limonite alteration with vuggy spaces that contain sulfides (C), to milky white and brecciated (D).

4.2 GEOLOGIC MAPS AND CROSS SECTIONS

Geologic, limonite intensity, and structural maps were prepared and modified from field maps using ArcMap 10.2 and Adobe Illustrator. Finalized maps are at a scale of 1:7,500, and are divided into a northern and southern sector (Figures 4.4 – 4.6, and 4.7 – 4.9).

Cross sections were created from collected field data and structural measurements. Lines of section were chosen to best represent important mineralization trends; lines of section cut orthogonal to vein trends, thus no apparent dip needs to be accounted for, except for the Don Victor trend, which runs at an oblique angle to cross section line B – B′. Figures 4.4 and 4.7 show the lines of section, labeled from north to south, A – A′, B – B′, C – C′, and D – D′, respectively. Mineralized veins are represented in red on cross sections; veins at depth are solid where known trends exist, and dashed where mineralization is inferred or has potential for further prospect, but remains currently unexplored. Note that no form-lines exist in cross section due to a lack of foliation throughout the pluton.

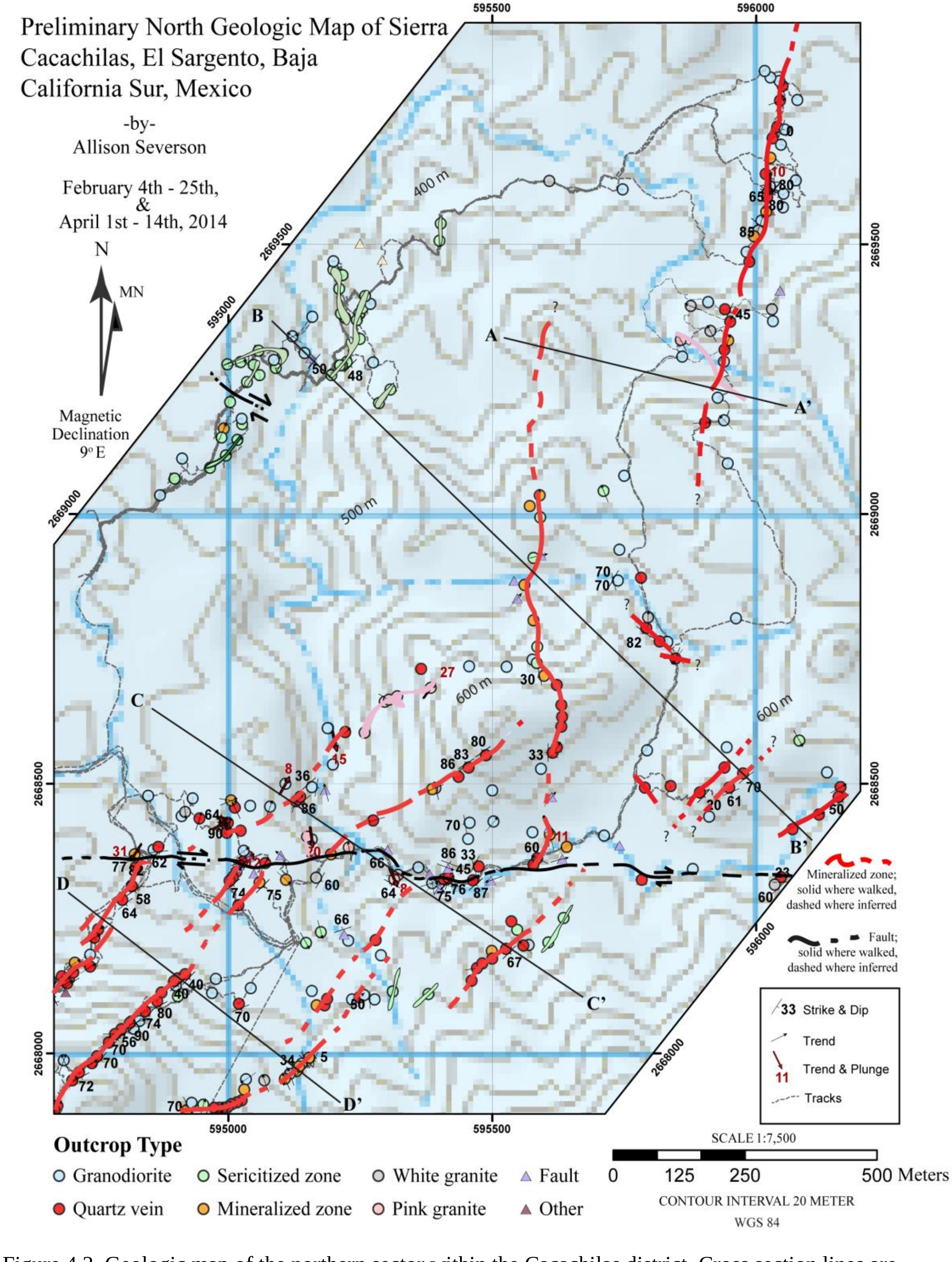

Figure 4.2. Geologic map of the northern sector within the Cacachilas district. Cross section lines are denoted by A-A′ through D-D′ lines of section that run perpendicular to mineralization.

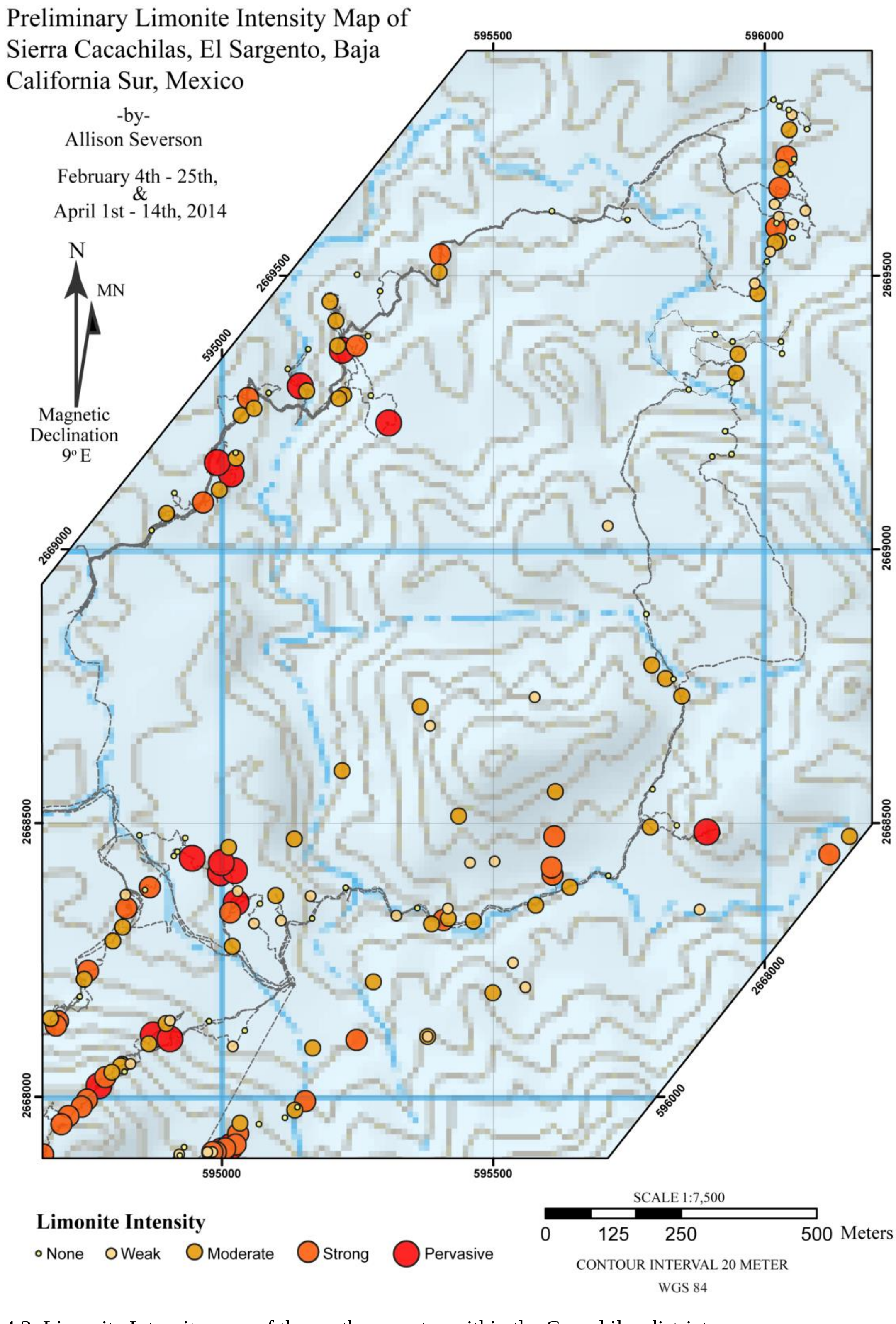

Figure 4.3. Limonite Intensity map of the northern sector within the Cacachilas district.

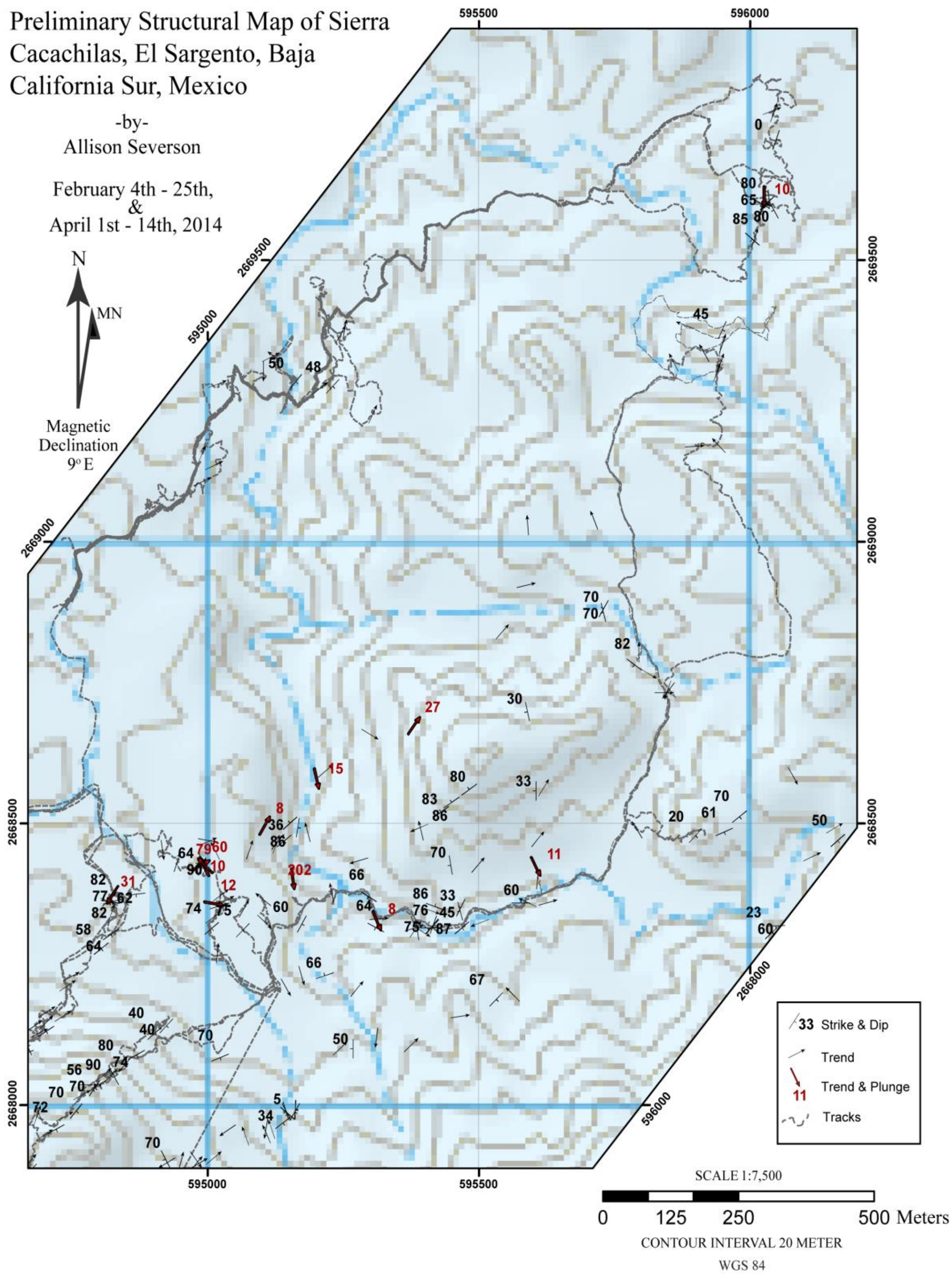

Figure 4.4. Structural map of the northern sector within the Cacachilas district.

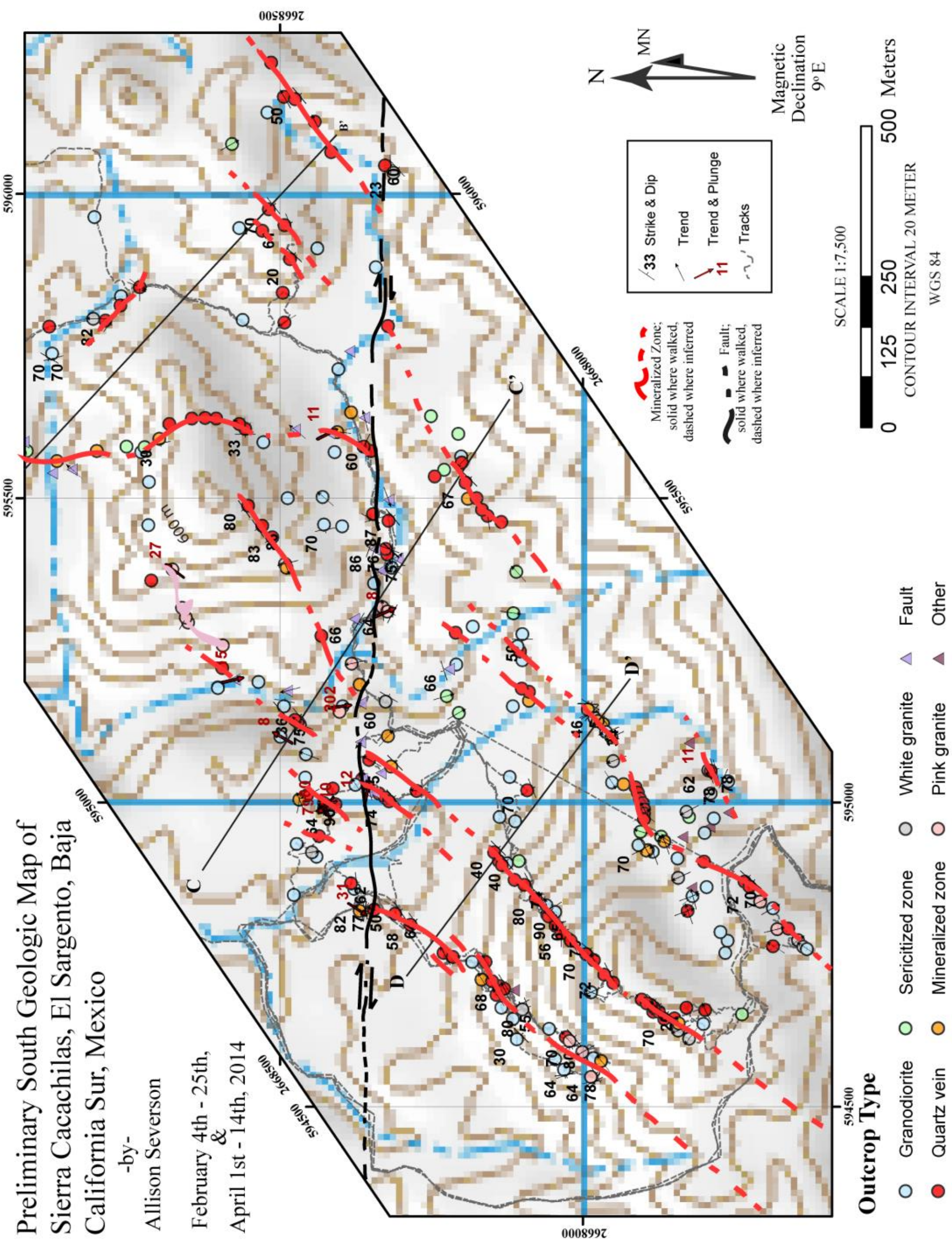

Figure 4.5. Geologic map of the southern sector within the Cacachilas district. Lines of section run perpendicular to mineralization trends.

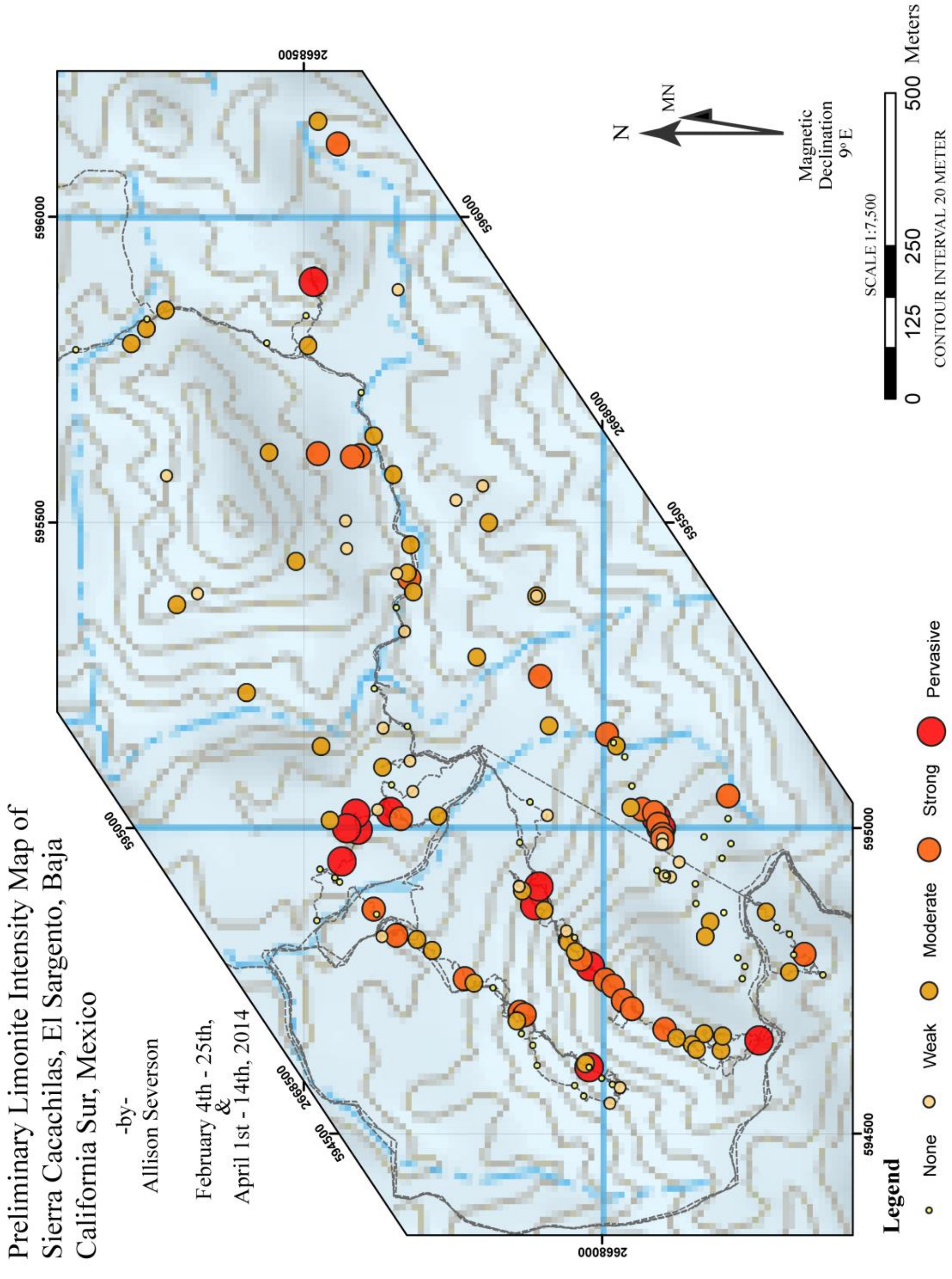

Figure 4.6. Limonite intensity map of the southern sector within the Cacachilas district.

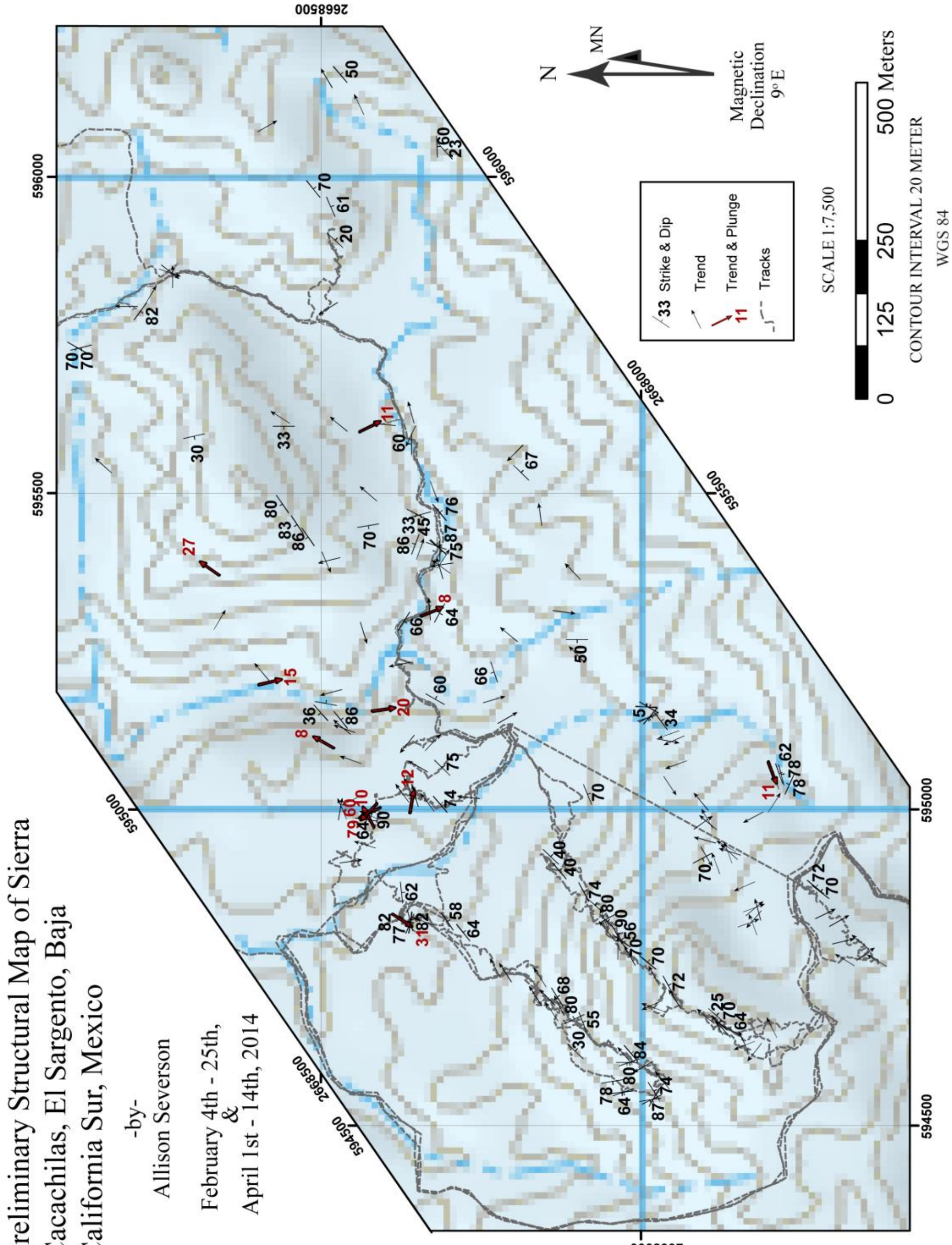

Figure 4.7. Structural map of the southern sector within the Cacachilas district.

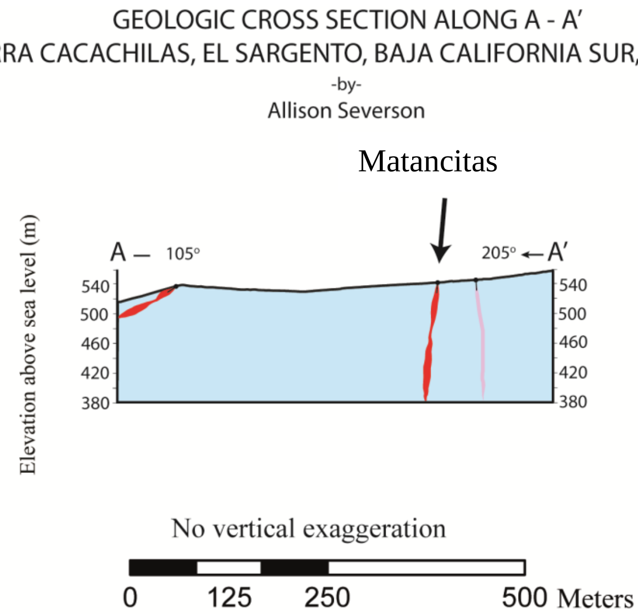

Figure 4.8. Geologic cross section A – A′.

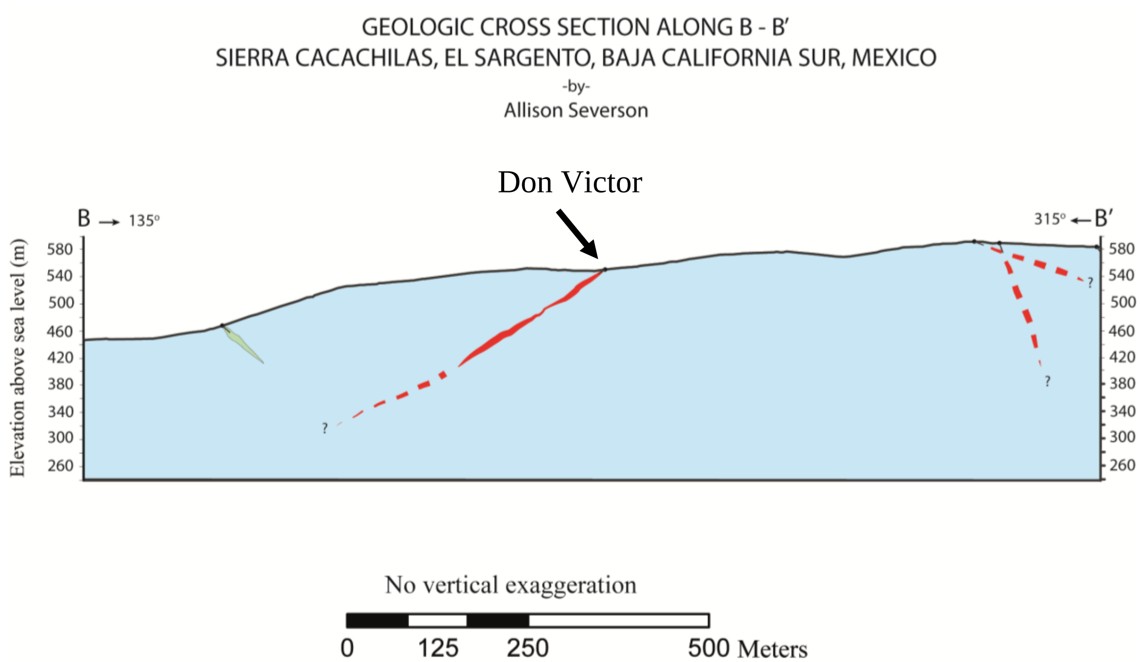

Figure 4.9. Geologic cross section B – B′.

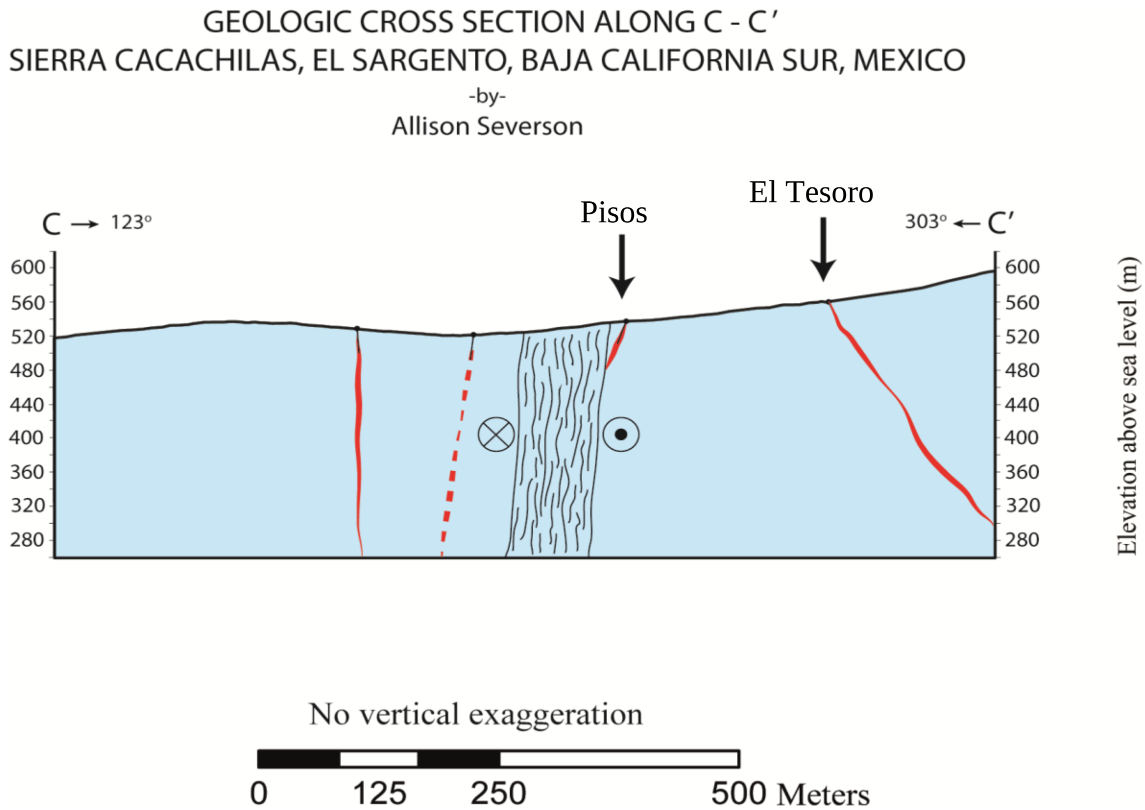

Figure 4.10. Geologic cross section C – C′.

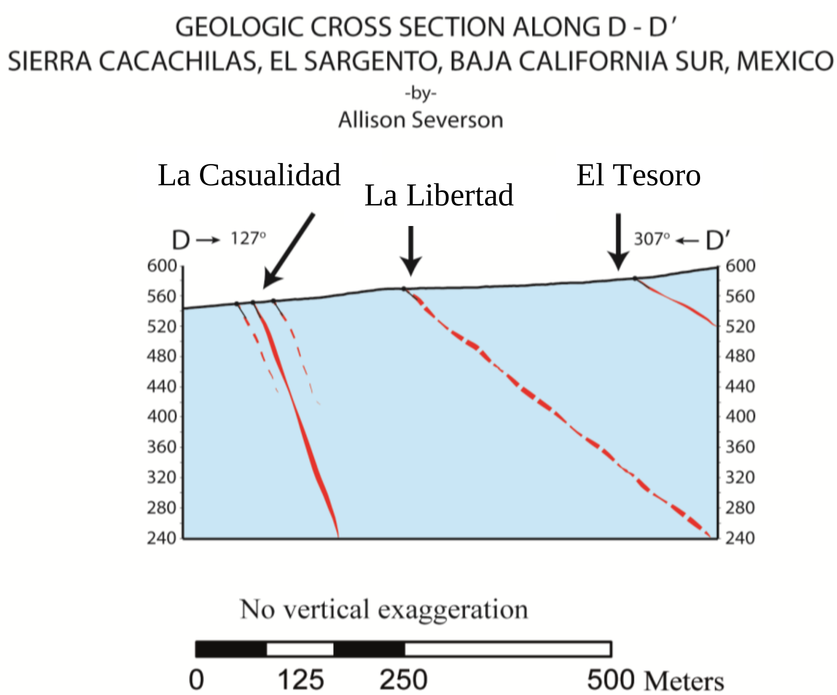

Figure 4.11. Geologic cross section D – D′.

4.3 GEOCHEMICAL RESULTS

Geochemical results presented in this section reflect field results as well as quantitative and qualitative assay returns of base and precious metals. Quantitative values of Au and Ag are left out for proprietary reasons, but reflect the same threshold values used in section 4.3 tables, Samuel Wachtor's thesis (unpublished), and figures herein (Figures 4.14 – 4.17; Appendix B). A brief summary is included here to provide preliminary geochemical insight on characteristics of the deposit; however, the area requires further geochemical studies to gain a more comprehensive understanding of the geochemistry of the pluton and related shear zones and greisen-like zones.

4.3.1 Mineralization-Related Alteration

Alteration of the pluton and mineralized zones is significant in determining potential economic viability at each location. There are several essential factors of alteration associated with relatively higher grades of mineralization. These alteration assemblages include: the breakdown and alteration of biotite and potassium feldspar to sericite; alteration of primary potassium feldspar to kaolinite and secondary potassium feldspar; prismatic quartz crystals and open space within quartz veins; subhedral to euhedral sulfide crystals associated with prismatic quartz crystals; and sulfides and metals forming along veinlets and microfractures. Associated with mineralized zones within the pluton, overprinting propylitic, kaolinitic, and silicic alteration occurs in the vicinity of greisen-like pods and mineralized quartz veins. All of these alteration types indicate an overall overprint of the country rock.

4.3.2 Limonite Alteration

Limonite alteration exists in the country rock in association with greisen-like and quartz vein mineralization. Limonite intensity of each mineralized trend is helpful in determining the economic potential at outcrop scale. Qualitative field analysis divides limonitic alteration into 5 distinct categories; none, weak, moderate, strong, and pervasive. Rocks with no or weak limonitic alteration typically have weak hematitic alteration along fractures and have insignificant amounts of Au or Ag. Rocks with moderate limonite alteration have hematitic alteration along fractures and crystal boundaries and also yield low Au and Ag values. Strong to pervasive amounts of limonitic alteration have intense hematitic and goethite alteration, and can even display box-work texture where potassium feldspars and sulfides have either been replaced or altered out of the rock, leaving behind a kaolinitic and strongly hematitic grunge. Rocks with strong to pervasive limonite alteration typically report relatively high amounts of Au and Ag.

Limonite categories are mapped and plotted on limonite intensity maps (Figures 4.5 & 4.8) and correlate to geologic and structural maps. Limonitic alteration, in conjunction with controls on mineralization mentioned in the previous section (4.3.1), is useful in qualitatively analyzing individual mineralized trends to resolve whether or not specific locations along the trend are economic. It should be noted that while limonite intensity is helpful in determining the amount of mineralization at each location, other field and laboratory factors – potassic and sericitic alteration, sulfide abundance, assay results, etc. – need to be assessed at each locale.

4.3.3 Assay Results

Samples for assay were collected at outcrop locations that demonstrated economic potential. Gold and silver assay results are plotted qualitatively on regional maps of the Cacachilas district (Figure 4.14 & 4.15). These results represent personally collected samples and samples collected by Samuel Wachtor in previous exploration studies within the district. Geographically, gold and silver values associated with quartz vein mineralization decrease from west to east (Figures 4.14 - 4.17). Furthermore, lead, zinc, and copper values also decrease west to east (Figure 4.16 & 4.17). This indicates at least two possible options: either mineralization becomes more distal to the deposit and interacting fluids to the east, or that the metals and incompatible elements associated with the last gasps of pluton emplacement are focused towards the west. In either case, higher grades may lie to the west with an overall decrease in precious and base metal values to the east.

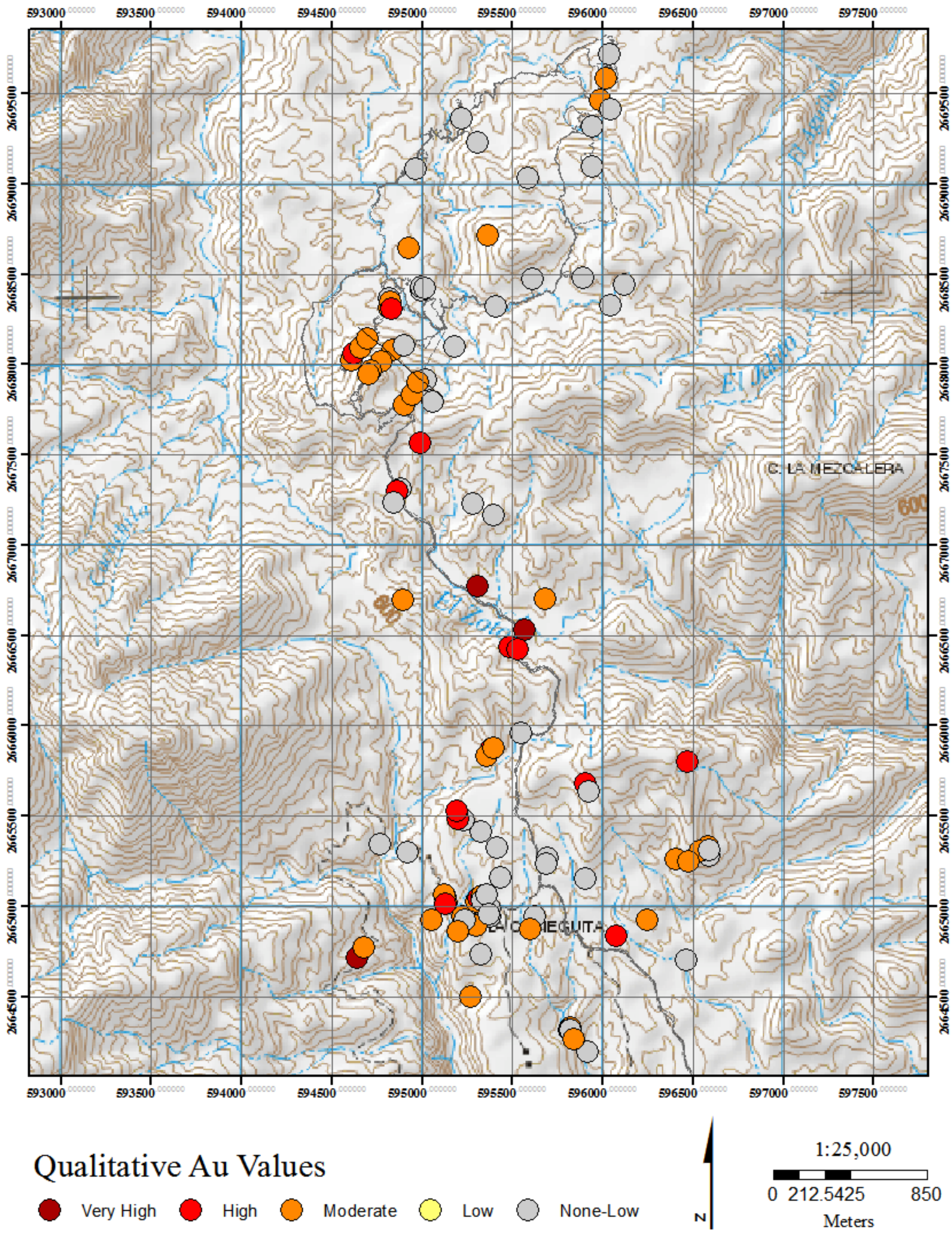

Figure 4.12. Qualitative Au values throughout the Cacachilas district from Severson (Appendix B) and Wachtor (unpublished) field data.

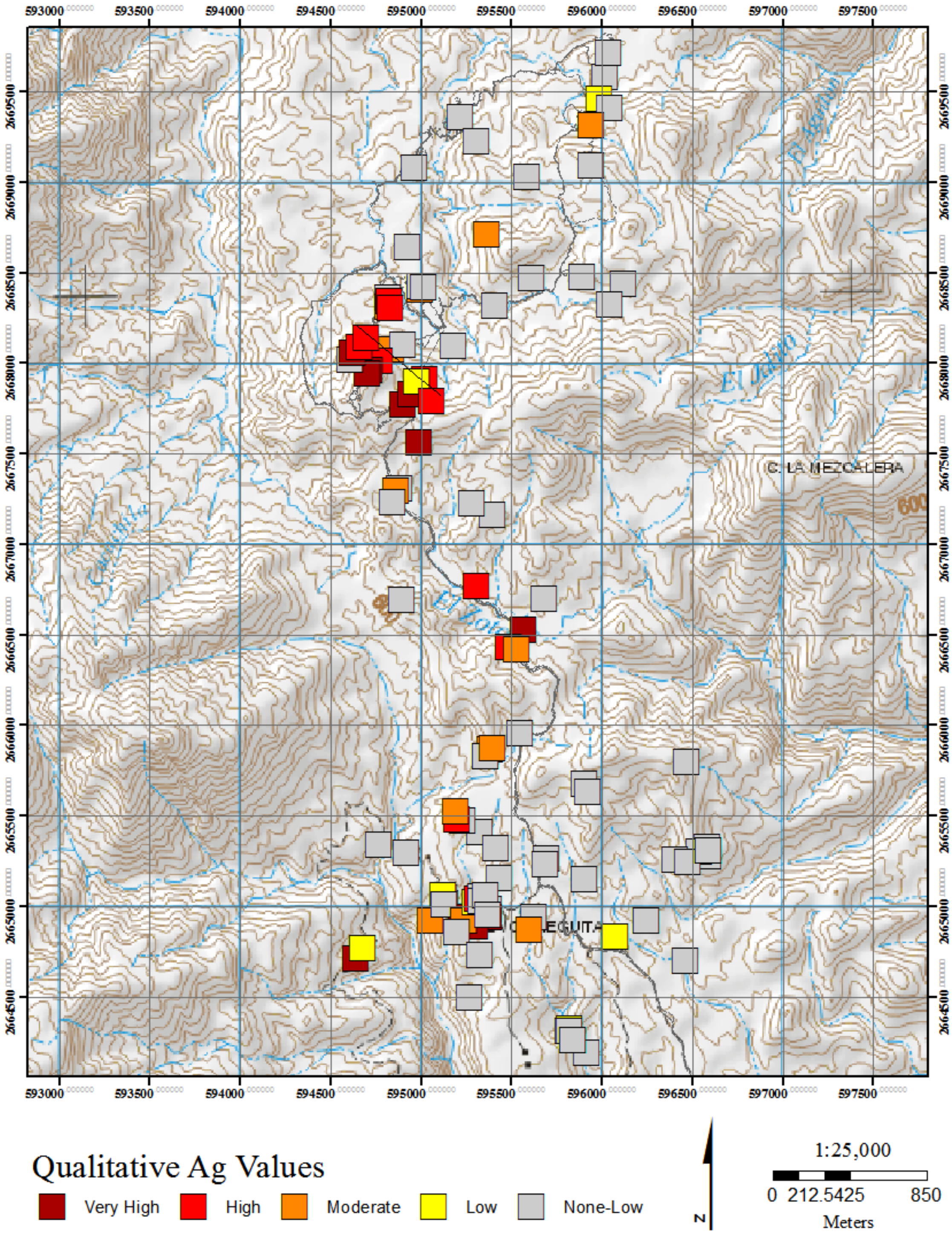

Figure 4.13. Qualitative Ag values throughout the Cacachilas district from Severson (Appendix B) and Wachtor (unpublished) field data.

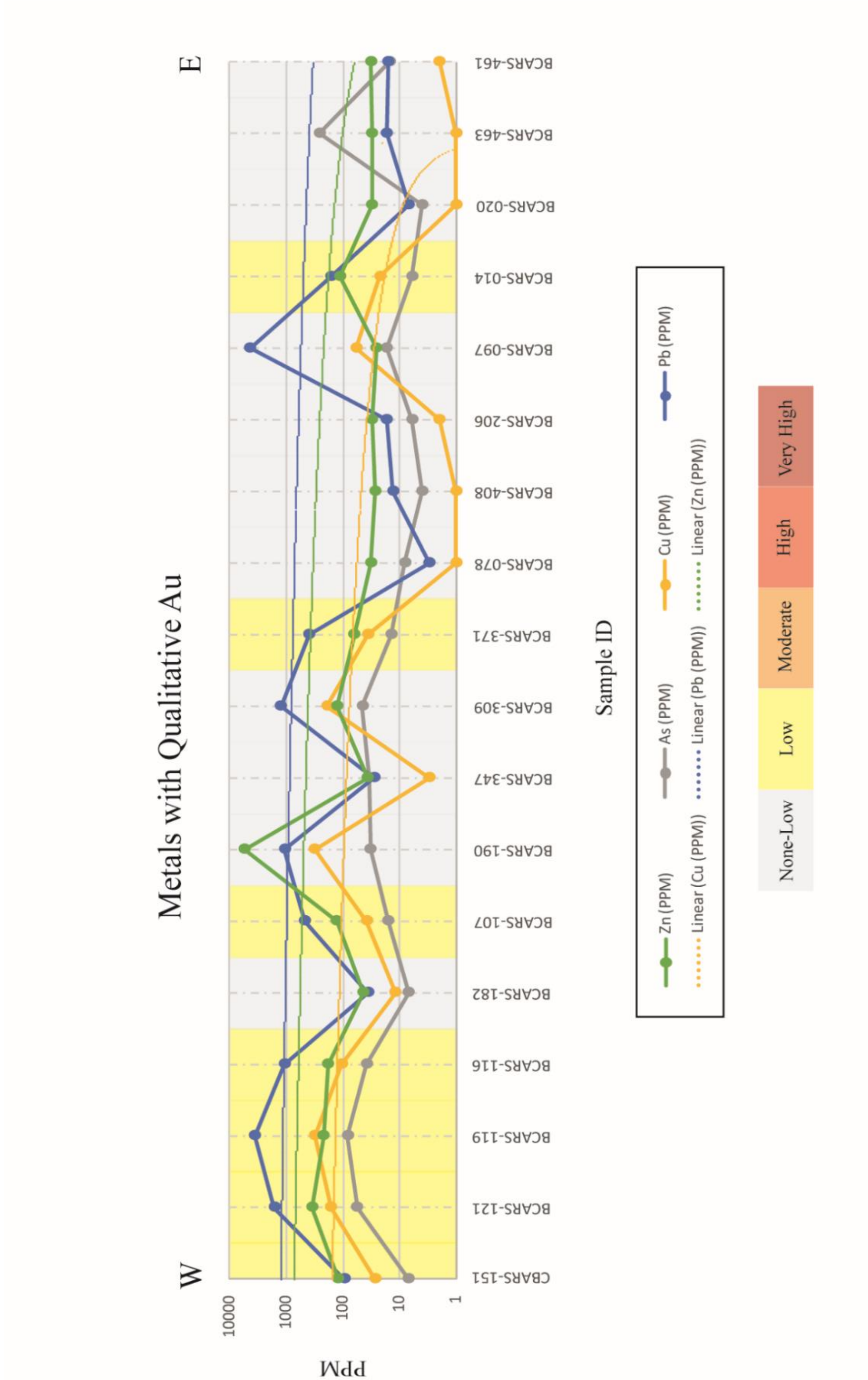

Figure 4.14. Assay values of quantitative Zn, As, Cu, and Pb and qualitative Au plotted logarithmically west to east. Zn, Cu, and Pb values decrease in PPM from west to east. Au values remain relatively low overall, but decreases in grade from west to east.

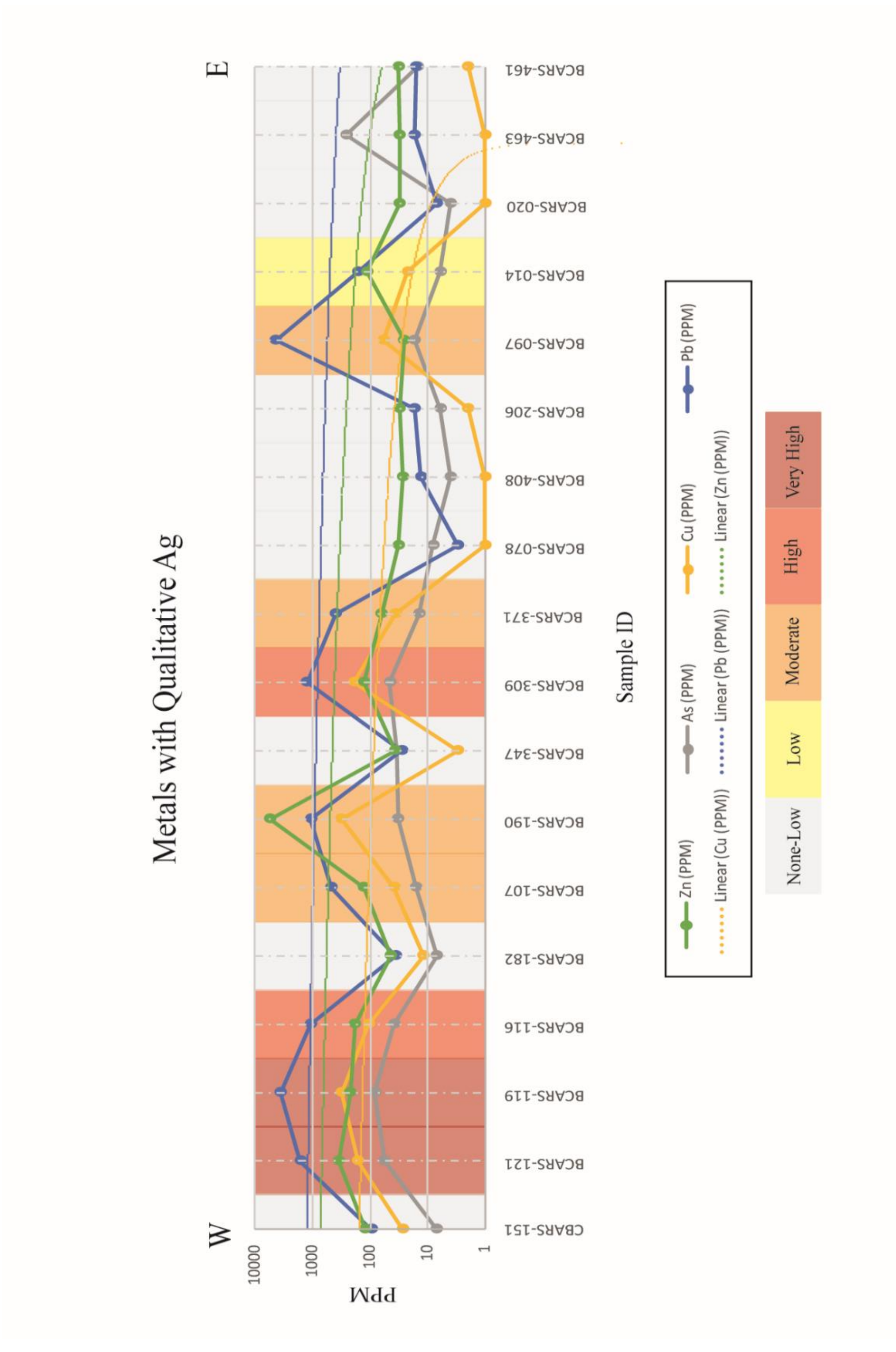

Figure 4.15. Assay values of quantitative Zn, As, Cu, and Pb and qualitative Ag plotted logarithmically west to east. Zn, Cu, and Pb values decrease in PPM from west to east. Ag values decrease from relatively "Very High" to "None to Low" grade from west to east.

4.4 STRUCTURAL RESULTS

This section presents field measurements and results relating to structural controls of the granodiorite, mineralized quartz vein trends, and greisen-like pods. No obvious foliation is noted in the granodiorite body. There are, however, two dominant orientations within the pluton. The first notable orientation that occurs within the pluton is represented by pink and white granite dikes; the second is the greisen-like pods and quartz veins. Pink and white dikes trend generally NNW (Figure 4.18), whereas the mineralized zones trend generally NE (Figure 4.19); this variation suggests a change in orientation of the principle stresses between the two events.

Mineralized veins and greisen-like podiform structures both trend northeast (Figure 4.19). Podiform structures are less poorly constrained than mineralized veins and trend 000^{o}-080^{o}. Mineralized shear zones strike approximately 045^{o} and dip mainly 65^{o}-85^{o} southeast, but local quartz veins within these systems trend 050^{o}-062^{o} suggesting a right-jogging en echelon array (Figure 4.20).

Brittle and brittle-ductile deformation is identified in the field area (Figure 4.21 & 4.22); ductile features are sparse and when located, are overprinted by brittle structures. Brittle deformation is dominant in the pluton, but variability from brittle to ductile features along any given trend makes it difficult to constrain potential prospects. Brittle-related features contain higher Au and Ag values than their brittle-ductile equivalents, and trends with promising strong limonitic and sericitic alteration reported low assay values when associated with brittle-ductile features.

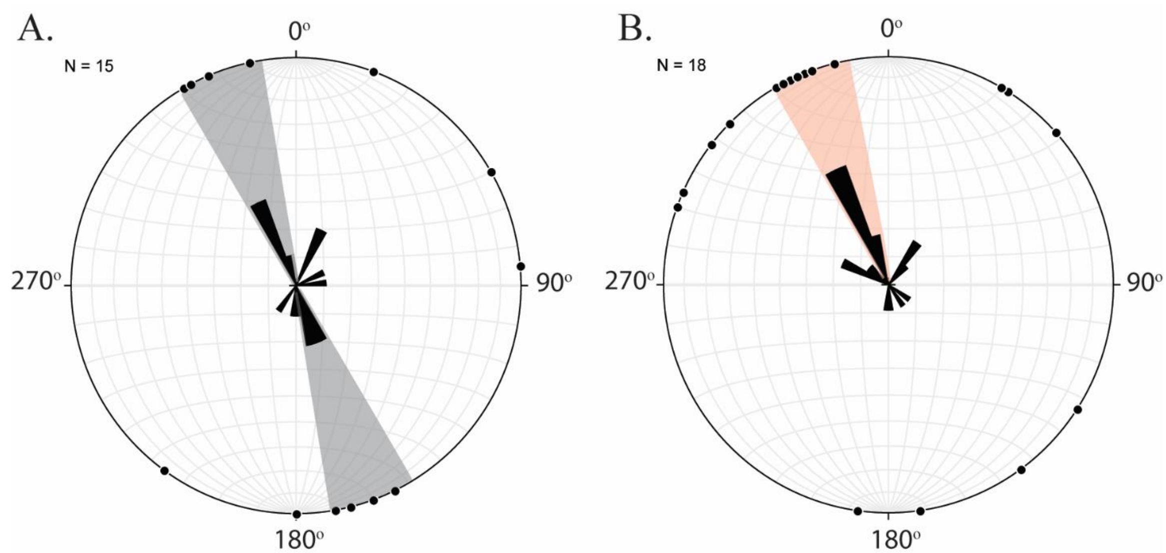

Figure 4.16. Rose-plot diagrams representing; (A) trends of white granite dikes, and (B) trends of pink granite dikes in the northern section of the Cacachilas district. General over-arching trend is north-northwest.

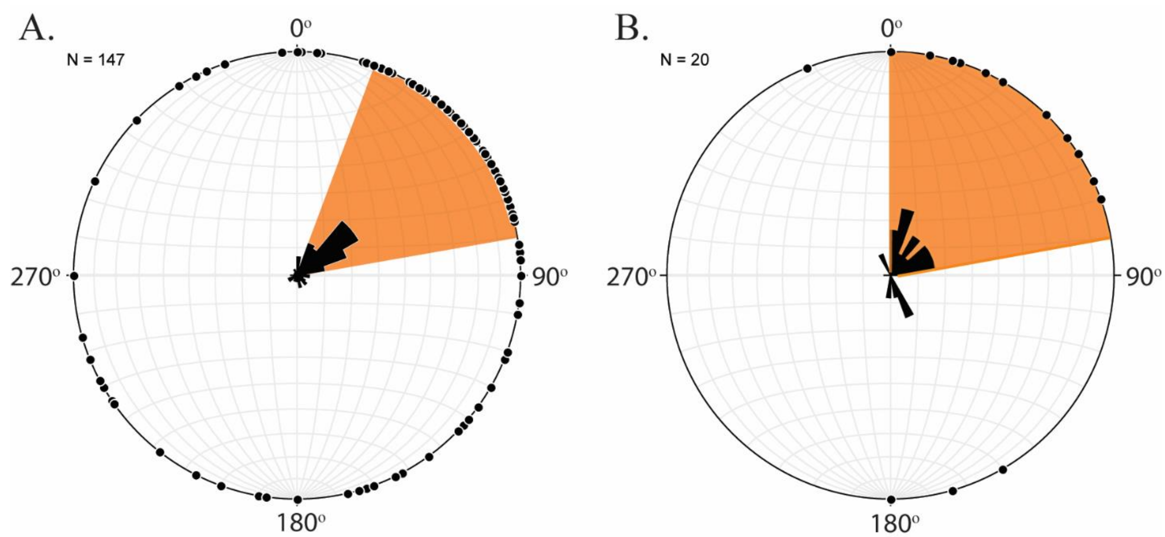

Figure 4.17. Rose-plot diagrams representing; (A) trends of quartz veins and mineralized veins, and (B) trends of greisen-like podiform structures in the northern section of the Cacachilas district. The general trend is northeast.

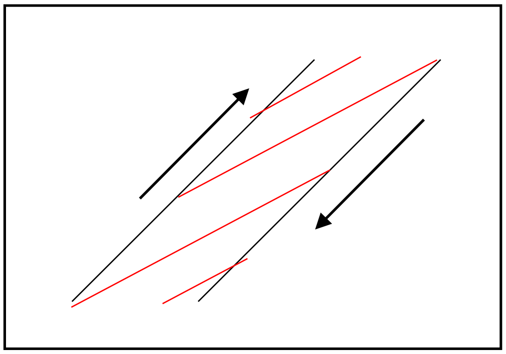

Figure 4.18. En echelon-style mineralization where black represents overall trend of vein systems and red represents individual quartz vein trends. This simplistic model represents a right-jogging, right-lateral stepping en echelon array that may control mineralization in the Cacachilas district.

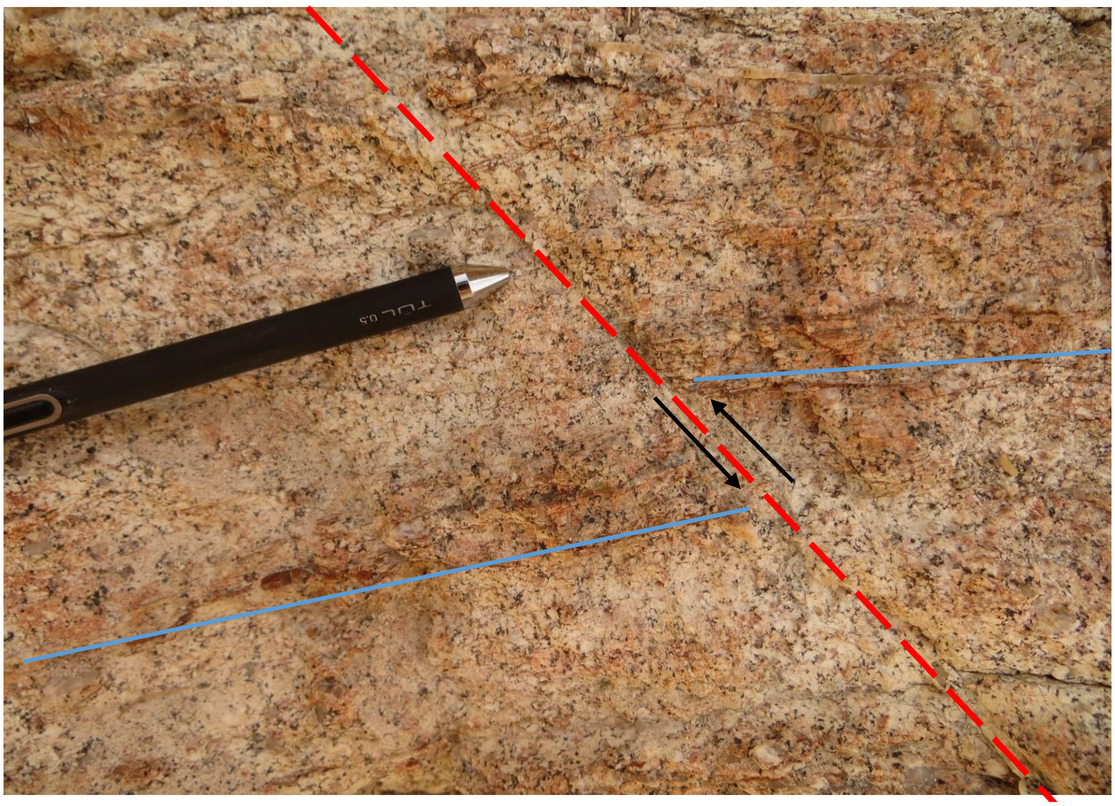

Figure 4.19. An example of brittle deformation within the granodiorite pluton.

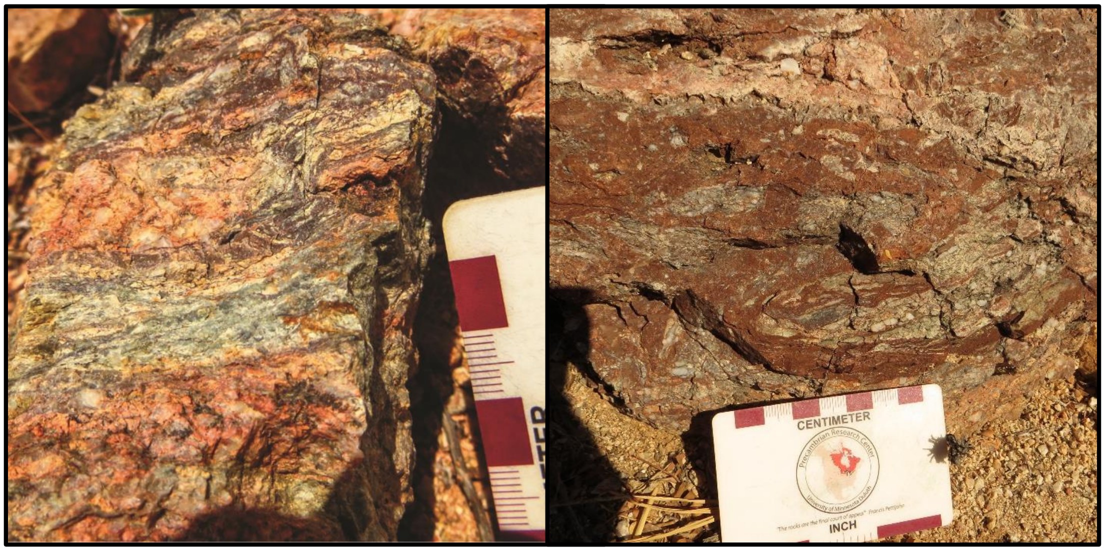

Figure 4.20. Examples of brittle-ductile deformation within the granodiorite pluton. Brittle-ductile deformation is overprinted by brittle deformation and is a poor host to mineralization.

4.5 DEPOSIT GEOLOGY

Historic and newly discovered trends within the northern section of the district (Figures 4.23 & 4.24) are classified into individual sections herein. Note that UTM coordinates provided for each trend are from southernmost to northernmost recorded extent of each mineralized system. Of particular interest along each prospective trend is the abundance of precious and base metals (Au, Ag, Cu, Pb, and Zn) as well as alteration and mineralization features that distinguish individual trends. These combined aspects will determine economic viability of the district as a whole, and will also determine where to focus exploration efforts on mineralized zones of relatively higher grade and potential.

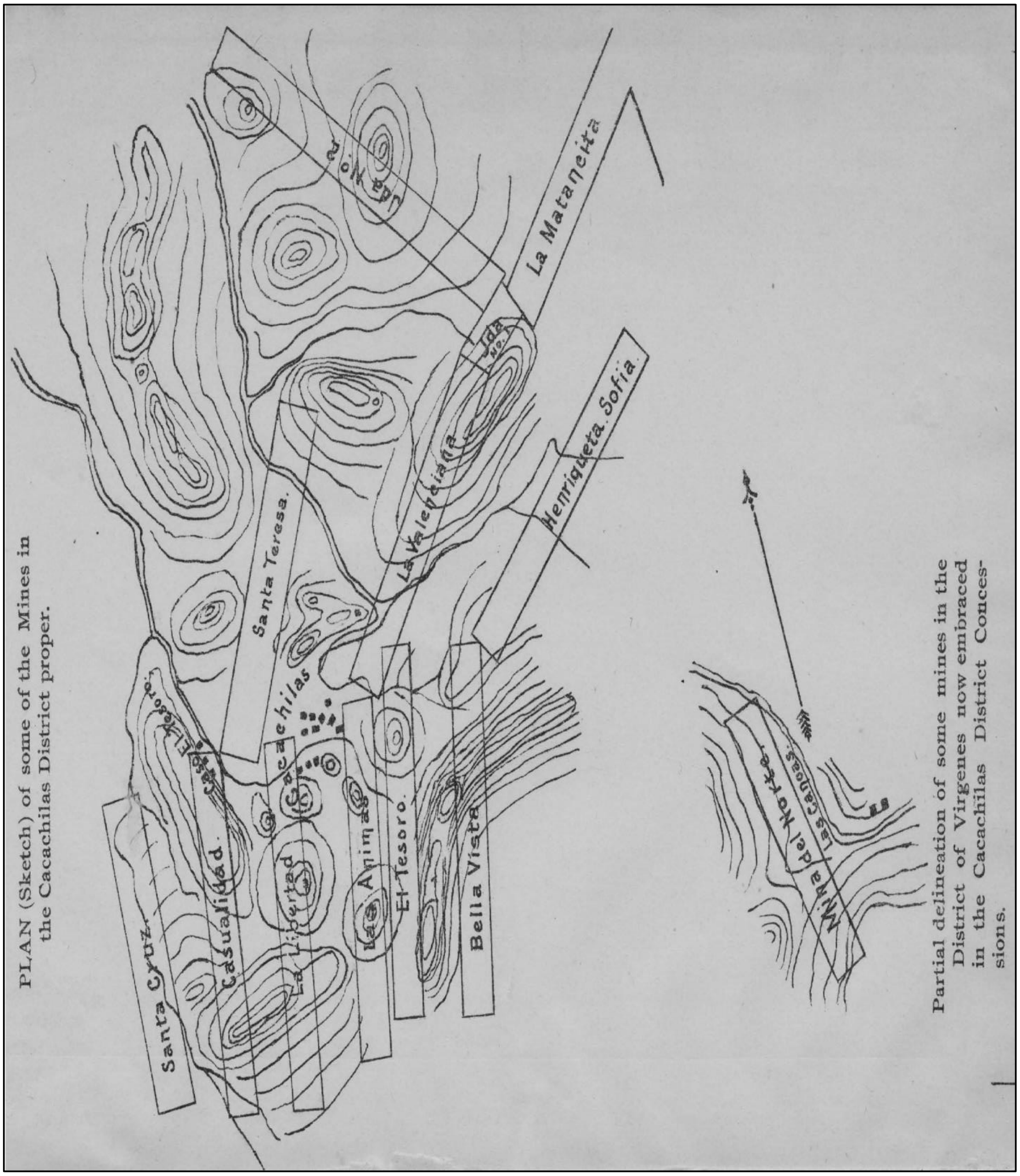

Figure 4.21. From Orynski (1889) - Sketch by engineer Sr. Juan J. Matute of historic trends within the northernmost area of the Cacachilas district.

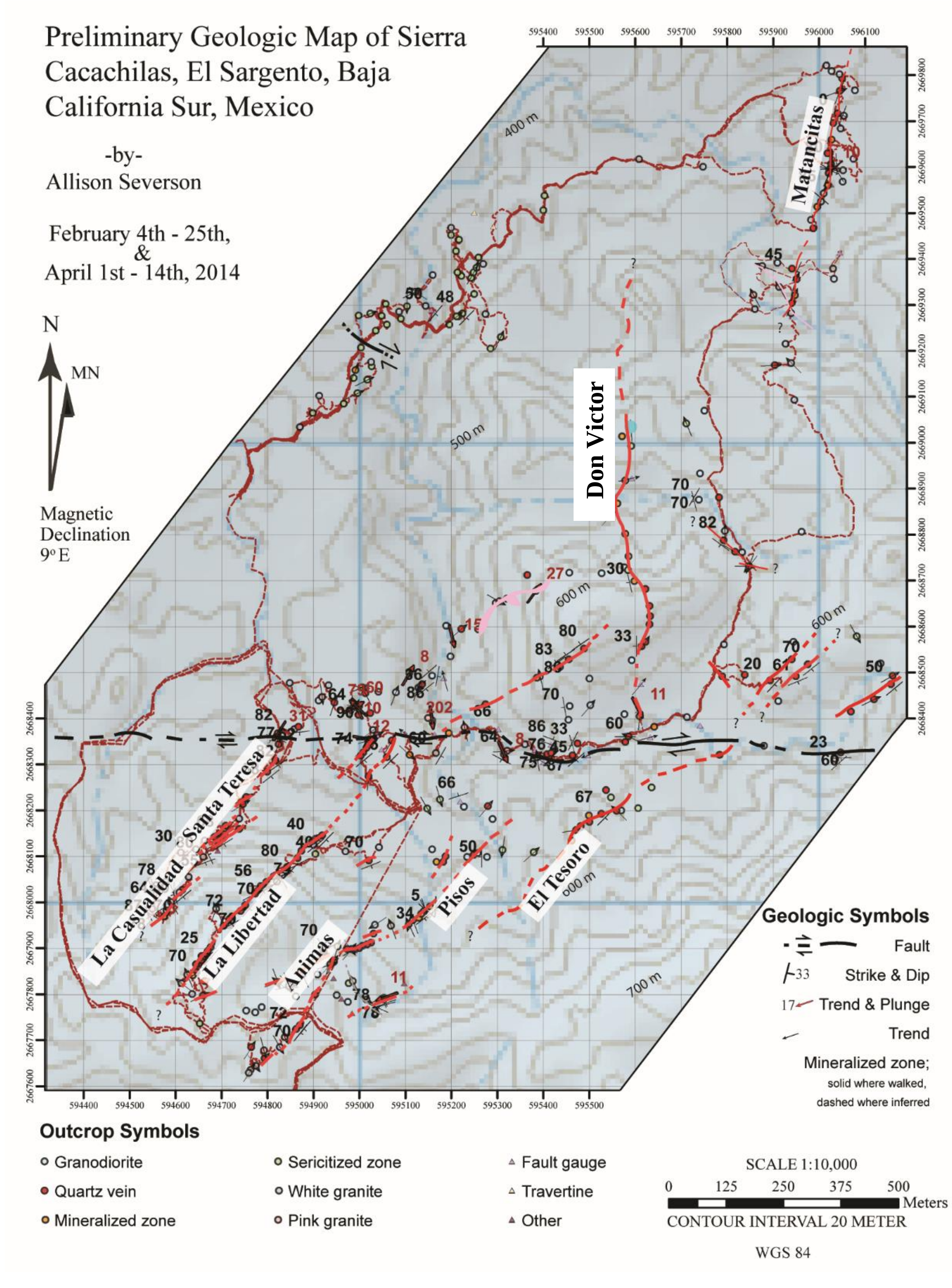

Figure 4.22. Prospective map of historic trends interpreted and modified from collected field data and maps, and from desriptions by Orynski (1889).

4.5.1 La Casualidad/Santa Teresa

[(594575, 2667970) to (594867, 2668383)]

The La Casualidad and Santa Teresa workings are located in the southwestern section of the field area (Figures 4.23 & 4.24) and represent a northeast-trending vein system. La Casualidad encompasses the southern end, whereas Santa Teresa represents the northern end of the trend before it is truncated along the main right-lateral fault that runs through the central portion of the field area. The La Casualidad-Santa Teresa networking vein system has an orientation of 045º; however, local quartz veins within the system strike 050º-062º and dip 55º-70º southeast, suggesting an en echelon style array of mineralization (Figure 4.20). Three minor quartz vein trends are parallel and make up the southern end of the mineralized trend, thereby representing La Casualidad. At the northern end of the trend (Santa Teresa), quartz veins become very thin discontinuous; quartz is glassy in texture and fills fractures that are <1 to 2 mm in width. Milky white quartz veins along trend (Figure 4.25) range 0.5 to 3 cm in width with trace amounts (<2-4%) of sulfides. Relic pyrite cubes are peppered along the contact between quartz vein and granodiorite, and are 1-4 mm in diameter.

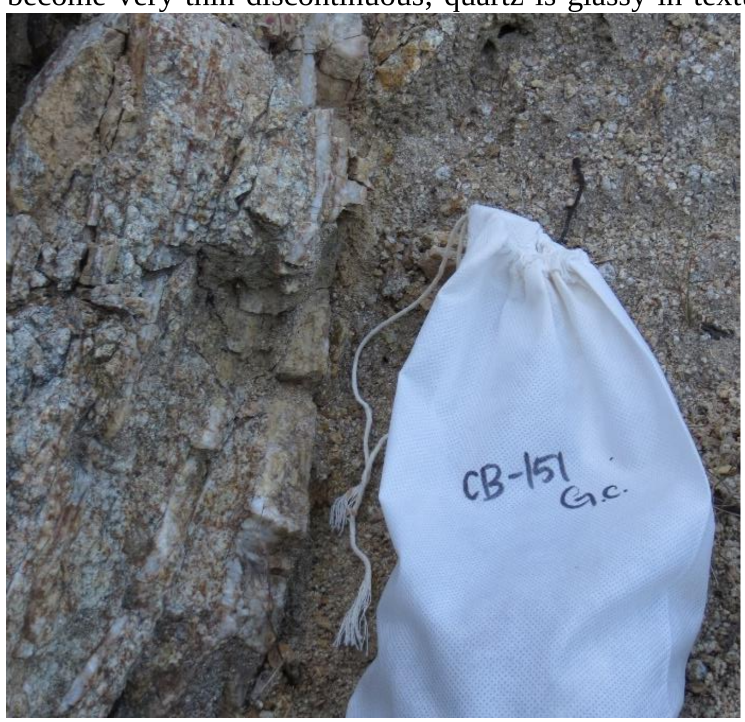

Figure 4.23. Photo of a sample collected from the La Casualidad and Santa Teresa trend. Note that quartz veins are milky white and range approximately 1-2 cm in width.

Limonitic alteration is weak on fresh surfaces with locally strong to pervasive alteration surrounding relic sulfides. Weak to moderate sericitic alteration is variable, but present along trend. Little to no evidence of open space quartz veins is present. Silver values along the Casualidad and Santa Teresa trend are generally high, while gold values are variable along trend (Table 1).

Sample ID	**Northing**	**Easting**	**Au**	**Ag**	**Cu (PPM)**	**Pb (PPM)**	**Zn (PPM)**
BCARS -151	594203	2668022	Low	None-Low	27	14	30
133-526	594622	2668061	High	Very High	1105	5600	499
134-525	594660	2668091	Low	High	190	3570	215
134-528	594697	2668142	Moderate	High	128	2040	277
134-588	594834	2668307	High	High	2570	>10000	3970
133-522	594822	2668314	Low	Moderate	187	501	526
134-582A	594826	2668347	Low	None-Low	12	53	135
134-582B	594826	2668347	Moderate	High	2970	>10000	9800
BCARS -182	594822	2668369	None-Low	None-Low	12	36	44

Table 1. Collected samples for assay along the La Casualidad and Santa Teresa trend with provided qualitative and quantitative precious and base metal values.

4.5.2 La Libertad

[(594637, 2667842) to (594918, 2668147)]

La Libertad runs parallel to and lies just east of La Casualidad and Santa Teresa (Figures 4.23 & 4.24). La Libertad veins are variable along trend; some sections of La Libertad are intensely silicified (Figure 4.26), whereas other sections are milky, open-space quartz veins with sericitic alteration. However, La Libertad is distinguishable by its milky white quartz veins that range from 1 cm to 20 cm in width. Trace to abundant (<2% - 5%) metallic blue-black sulfides form in minor vuggy spaces within prismatic quartz veins. Supergene-enriched malachite and azurite are present, but sparse, only forming when sulfides are 5% or greater within quartz veins. La Libertad quartz veins are similar to La Casualidad and Santa Teresa, but limonite and sericitic alteration are stronger on the La Libertad trend. Limonite alteration is strong to pervasive, primary potassium feldspar has broken down to sericite, and secondary potassium feldspar is locally present along sericitic veinlets (<1 cm), indicating potassic alteration overprinting this vein system. Sericite replaces biotite locally, but biotite remains fairly stable overall, and forms short stacks ≤2 mm in height. Also present, albeit sparse, are epidote veins; these appear to have little to no effect on mineralization. Overall, La Libertad trends 045^{o}, whereas individual quartz veins within the system range in strike from 040^{o}-062^{o} and dip 40^{o}-70^{o} southeast, suggesting a right-stepping en echelon array. Brittle overprint occurs in the northern end of the La Libertad trend; this may be associated with uplift or formation of the right-lateral strike-slip fault during or shortly after mineralization. The high abundance of sulfides, local presence of supergene malachite and azurite, and grade return of Au and Ag assay results (Table 2) make La Libertad a very promising trend.

Sample ID	**Northing**	**Easting**	**Au**	**Ag**	**Cu (PPM)**	**Pb (PPM)**	**Zn (PPM)**
BCARS-121	594704	2667950	Low	Very High	164	1610	350
BCARS-119	594717	2667965	Low	Very High	315	3620	223
BCARS-116	594773	2668020	Low	High	105	1070	185
BCARS-107	594842	2668078	Low	Moderate	38	474	131
BCARS-109	594904	2668106	None-Low	None-Low	14	13	30

Table 2. Collected samples for assay along the La Libertad trend with provided qualitative and quantitative precious and base metal values.

Figure 4.24. An example of quartz veins along the La Libertad trend. This outcrop is intensely silicified, making it difficult to sample, but high presence of sulfides and a sample return of high Ag values make this a promising trend.

Figure 4.25. (SAMPLE CBARS-309) Sample representing strong to pervasive limonite intensity with an abundance of visible Cu- & Au-related mineralization. This location ran very high in Ag, and moderately to very high in Au.

4.5.3 Animas

[(594793, 2667661) to (594989, 2667899)]

Animas is located east of the La Libertad trend and west of the El Tesoro trend (Figures 4.23 & 4.24). Greisen-like alteration dominates the Animas trend with mineralized zones up to 20 cm in width. Euhedral pyrite is present in sparse open space quartz veins (Figure 4.27). The Animas zone strikes 035^o and dips 70^o southeast in the southernmost mapped extent, and bends eastward in the northernmost mapped area (Figures 4.23 & 4.24). Mineralization strikes approximately 060^o in the northern sector, following the same orientation as the Pisos vein to the northeast. Mineralization within the southern portion of the Animas vein system ranges in strike from 030^o to 040^o and reflects the overall 035^o trend in the southern portion, thus does not reflect en echelon style mineralization. Limonite alteration is weak to moderate in the southern portion of the trend, but increases after the easterly bend in the system. Sulfide abundance is very low (<1%) along the entire trend. Sericitic alteration is present along mineralized zones and associated fractures, thereby indicating that mineralization along this trend is greisen-like rather than dominated by quartz veins. It should be noted, however, that thin quartz veins (<2 cm in width) are locally present and have intense sericitic, and clay-rich alteration and strong limonitic alteration. Biotite is replaced locally, but remains unaltered overall. Gold returns for Animas are poor, but silver returns are high to very high (Table 3) along trend, indicating potential value for further development.

Sample ID	Northing	Easting	Au	Ag	Cu (PPM)	Pb (PPM)	Zn (PPM)
133-534	594900	2667777	Low	Very High	602	1970	847
133-540	594945	2667833	Low	Very High	166	2000	981
133-543	594979	2667901	Low	Low	39	218	157
BCARS-309	595025	2667913	None-Low	High	189	1265	127

Table 3. Collected samples for assay along the Animas trend with provided qualitative and quantitative precious and base metal values.

4.5.4 Pisos

[(594989, 2667899) to (595153, 2667992)]

Pisos lies northeast of Animas and west of El Tesoro, and after an easterly bend of mineralization appears to follow the same trend as Animas (Figure 4.23 & 4.24). Pisos is dominantly greisen-like, with minor amounts of milky quartz veins and sericitic replacement along joints and fractures. Mineralization is locally curviplanar but reflects an overall strike of 055^{o} and dip range of 65^{o}-80^{o} southeast. Quartz veins within the Pisos system reflect the orientation of mineralization, ranging from 051^{o} to 060^{o}. Limonite alteration along the Pisos trend is strong to pervasive overall, with localized weak to moderate limonite alteration. Secondary potassium feldspar and kaolinite is present with sericitic alteration; localized biotite alteration is present, with less than 5% of original biotite remaining. Sulfide abundance is trace overall, but is locally up to 5%. The Pisos trend yields high silver values, but it should be noted that mineralization along this trend is variable with anastomosing textures that alternate between greisen-like structures, open space milky quartz veins with pervasive sulfides, and sericitic-altered joints and fractures.

Thus, while silver values exhibit promise, further geochemical analysis needs to be achieved along this trend.

4.5.5 El Tesoro

[(595461, 2668135) to (595559, 2668200)]

El Tesoro lies east of Pisos and represents the easternmost mapped mineralized zone in the northern field area (Figures 4.23 & 4.24). El Tesoro has an orientation of approximately 045^o to 060^o and dip of 45^o-67^o southeast (Figure 4.28), and is subparallel to the Pisos trend. Mineralization is quartz vein dominant with intense sericitic alteration along the contact between quartz veins and granodiorite. Limonitic alteration is weak to moderate overall, but intense sericitic and clay alteration is present. Sulfides are trace (≤2%) and peppered along quartz veins. Similar to Pisos, El Tesoro mineralization is variable along trend; mineralization ranges from vuggy open space quartz veins to milky white quartz veins, to sericitic alteration along fractures to greisen-like alteration overall. Geochemical analysis of this trend will help determine areas of economic value.

Figure 4.26. Adit located along El Tesoro trend showing mineralization (outlined in red) with a southeast dip of 67^o. Adit opening is 1m in width.

4.5.6 Matancitas

[(595903, 2669170) to (596050, 2669794)]

The Matancitas trend is located in the northeastern-most extent of the field area (Figures 4.23 & 4.24). Matancitas has a more northerly orientation than previously discussed mineralized trends south of the main right-lateral fault; strike is approximately 020^{o}, with a subvertical dip ranging from 080^{o} east to 080^{o} west. Mineralization ranges 5 to 60 cm in width and is controlled by quartz veins with strong sericitic alteration. Quartz veins range from vuggy open space to milky white and are approximately 1-4 cm in diameter. Limonite and sericitic alteration is moderate to strong. Biotite is altered and replaced by sericite along the entire trend. Trace abundance of metallic dark blue-black sulfides and pyrite (≤3%) are peppered throughout veins, and form prismatic crystals in vuggy open space quartz veins. Matancitas mineralization is highly variable along trend with none to moderate amounts of Au and Ag (Table 4). Thus geochemical analysis along the trend is recommended to see if any areas are valuable enough to explore further.

Sample ID	**Northing**	**Easting**	**Au**	**Ag**	**Cu (PPM)**	**Pb (PPM)**	**Zn (PPM)**
BCARS -216	595946	2669094	None-Low	None-Low	2	29	28
BCARS -097	595947	2669322	None-Low	Moderate	58	4410	26
BCARS -093	596045	2669415	None-Low	None-Low	1	15	61
BCARS -014	595987	2669468	Moderate	Low	22	162	113
BCARS -004	596021	2669588	Moderate	None-Low	22	67	56
BCARS -020	596040	2669718	None-Low	None-Low	1	7	31

Table 4. Collected samples for assay along the Matancitas trend with provided qualitative and quantitative precious and base metal values.

4.5.7 Don Victor Prospect

[(595614, 2668558) to (595590, 2669035)]

A potential site of interest was located southwest of Matancitas and north of El Tesoro (Figure 4.24). This prospect, tentatively named the Don Victor Prospect, has a northerly strike of approximately 000º and a shallow dip of about 033º to the west. Assay returns are few and unfavorable (Table 5), but a more detailed analysis of the trend should be considered. Though the strike and dip vary from other trends in the Cacachilas district, suggesting a different, and likely later, emplacement orientation and process, this trend may provide answers to emplacement mechanisms of mineralized trends, and may also host mineralization. Prospect pits were located along this trend, but were sparsely spaced, indicating this is likely low grade.

Lack of mineralization may be due to lack of fluid mobility; cherty quartz veins are present instead of vuggy open space quartz veins, sulfides are very low (<<1%) to non-existent, limonite alteration along trend is weak to moderate overall and locally strong, and a large portion of alteration along trend displays weak sericitic alteration and moderate strong hematization instead. Evidence of brittle-ductile deformation is scarce, but present; thus, mineralization is likely poorly controlled in these areas. Furthermore, along the entire traverse of this structure, variation from highly jointed with slight sericitic alteration to intensely chewed up and altered granodiorite to quartz veins to greisen-like shear zones indicates a poorly constrained fluid pathway.

Sample ID	Northing	Easting	Au	Ag	Cu (PPM)	Pb (PPM)	Zn (PPM)
BCARS-391	595612	2668476	None-Low	None-Low	1	18	29
BCARS-408	595590	2669035	None-Low	None-Low	1	13	27

Table 5. Collected samples for assay along the newly discovered trend with provided qualitative and quantitative precious and base metal values.

5. DISCUSSION

5.1 OVERVIEW

This section discusses potential control(s) on and classification of the Cacachilas district. Structural constraints, similarities and differences from epithermal and mesothermal style deposits, and a comparison with other deposits situated throughout the LCB are combined to synthesize the deposit style within the Sierra Cacachilas.

5.2 STRUCTURAL CONTROLS

There are two main structural controls and inferred events of mineralization; the first event is responsible for greisen-like alteration of the granodiorite-tonalite host rock, the second event is responsible for quartz-vein emplacement. While these events are differentiable, it should be noted that both likely occurred episodically, as do fluid-assisted seismic events. This episodic movement would account for anastomosing shear zones and sericitic pods that pinch out along trend.

The first mineralization event is associated with greisen-like podiform structures and is interpreted to have occurred at higher pressures and greater depths under ductile to brittle conditions. During the initial mineralization phase, fluid pressure is interpreted to be dominantly responsible for rock failure, while confining pressure remained constant. Alternatively, differential stresses (σ_1 - σ_3) remained relatively unchanging, while fluid pressure increased (Figure 5.1). Fluids responsible for rock failure were potassium rich during the first period of mineralization and were likely associated with conditions similar to greenschist facies with metamorphic and/or magmatic fluids. Increase in fluid pressure is regarded as dominating rock failure, thus differential stress between the strongest principle stress (σ_1) and weakest principle stress (σ_3) could fluctuate, inferring variability in orientation of greisen-like trends. Fluid-pressure assisted tensile failure was likely the dominant process during this first mineralizing event.

The second mineralization event is associated with quartz and mineralized veins and is interpreted to have occurred at lower pressures and relatively shallower depths under brittle-ductile to brittle conditions. During this second phase of mineralization, an episodic increase in differential stress (σ_1- σ_3) associated with seismic build up and propagation along pre-existing fractures, was likely responsible for rock failure. Mineralization was dominantly silicic and less sericitic and potassic during the second event; albeit, potassic alteration is still noted by kaolinite, and secondary potassium feldspar alteration surrounding the quartz veins. This second event involved more faulting than did the greisen-like event, but tensile failure still occurred to form en-echelon quartz veins.

Brittle-ductile shear zones and low permeability of the granodiorite-tonalite pluton suggest formation and mineralization at depths that are less than 10-15 km (Robb, 2005), or no lower than the Brittle-Ductile Transition Zone (BDT). Given the anastomosing pattern of the shear zones, propagation was likely episodic with fracture rupture occurring along high-permeability conduits when either fluid pressure (P_f) or confining pressures exceeded the least principal stress (σ_3) (Sibson, 1998); in the case of the Sierra Cacachilas, σ_3 is in the north-northwest direction. A sudden change in the tectonic stress field would likely have caused major episodes to redistribute fluids (Sibson, 1998). This major episode may be marked in the Sierra Cacachilas by the change in orientation of stresses after emplacement of pink and white aplitic granite dikes and before greisen-like zones and quartz veins.

Formation of many deposits, including epithermal and mesothermal deposits, is controlled in-part by fault-driven fluid flow (Sibson, 1998). Veins and associated gold mineralization tend to form episodically during tectonic events, with dynamic fault-valve motion causing fluids to move upward along structures at or above the brittle ductile transition (Bierlein & Crowe, 2000). Sibson et al. (1975) discuss two main fluid flow models that could occur under certain pressure-temperature and crustal conditions. The seismic pumping model occurs at shallow depths, under epithermal-style conditions, while the fault-valve model occurs under higher pressures, deeper in the crust, and under mesothermal-style conditions.

Seismic pumping describes a theoretical model where cyclical stress variations associated with an active fault system promotes fluid flow (Sibson, 1975). Friction builds up in the rock along a pre-weakened zone; as shear stress increases around the fault, cracks form, creating fluid movement along pathways. As fault failure initiates, fluid pressures fall, and rupture along the fault occurs. Once rupture occurs, shear stress significantly drops and fluid pressure increases forcing fluids upward along the fault (Robb, 2005; Sibson, 1975). Shear stresses will start to rebuild, causing the cycle to repeat itself along the same channel-ways, allowing for multiple episodes of rupture and resultant mineralization and mobilization of fluids. The formation of open-space quartz veins at deeper crustal levels and the discharge of fluid into these open spaces results in rapid fluid pressure drop. Within 2-3 km of the surface, this pressure drop may also be explained by fluid boiling. Mechanical energy released by boiling could result in more fracturing and brecciation, allowing for an increase in fluid circulation and mineral precipitation (Robb, 2005).

Conversely, the fault valve model represents mesothermal-style deposits and may explain some high-angle reverse faults (Sibson, 1998). In a horizontally compressive stress regime, reactivation of high-angle faults can only occur when fluid pressure exceeds lithostatic load (Figure 5.1). Fault rupture occurs as fluid pressures achieve equivalent or greater levels than lithostatic load; as the fault fails and shear stresses are reduced, fault rupture allows for fluid discharge into the newly formed open space. Creation of open space forms by a dramatic decrease in fluid pressure, which allows for precipitation of minerals that cause the fault to essentially reseal itself (Robb, 2005). Upon resealing, fluid pressures will begin to increase again, allowing for the cycle to repeat itself.

The Sierra Cacachilas granodiorite-tonalite pluton acts as a natural impermeable unit that constrains fluid pathways along weakened zones. The low permeability and high pressure of the pluton during shearing is interpreted to have confined fluid pathways to small meter-wide shear zones. At depth (>4 km), as pore fluid pressure increased, the granodiorite eventually fractured allowing for metasomatic fluids to alter the surrounding rock from pristine granodiorite to an altered sericitic greisen-like pod. The poorly constrained trends of greisen-like podiform structures (Figure 4.19B) indicate a high fluid pressure and relatively low differential stress.

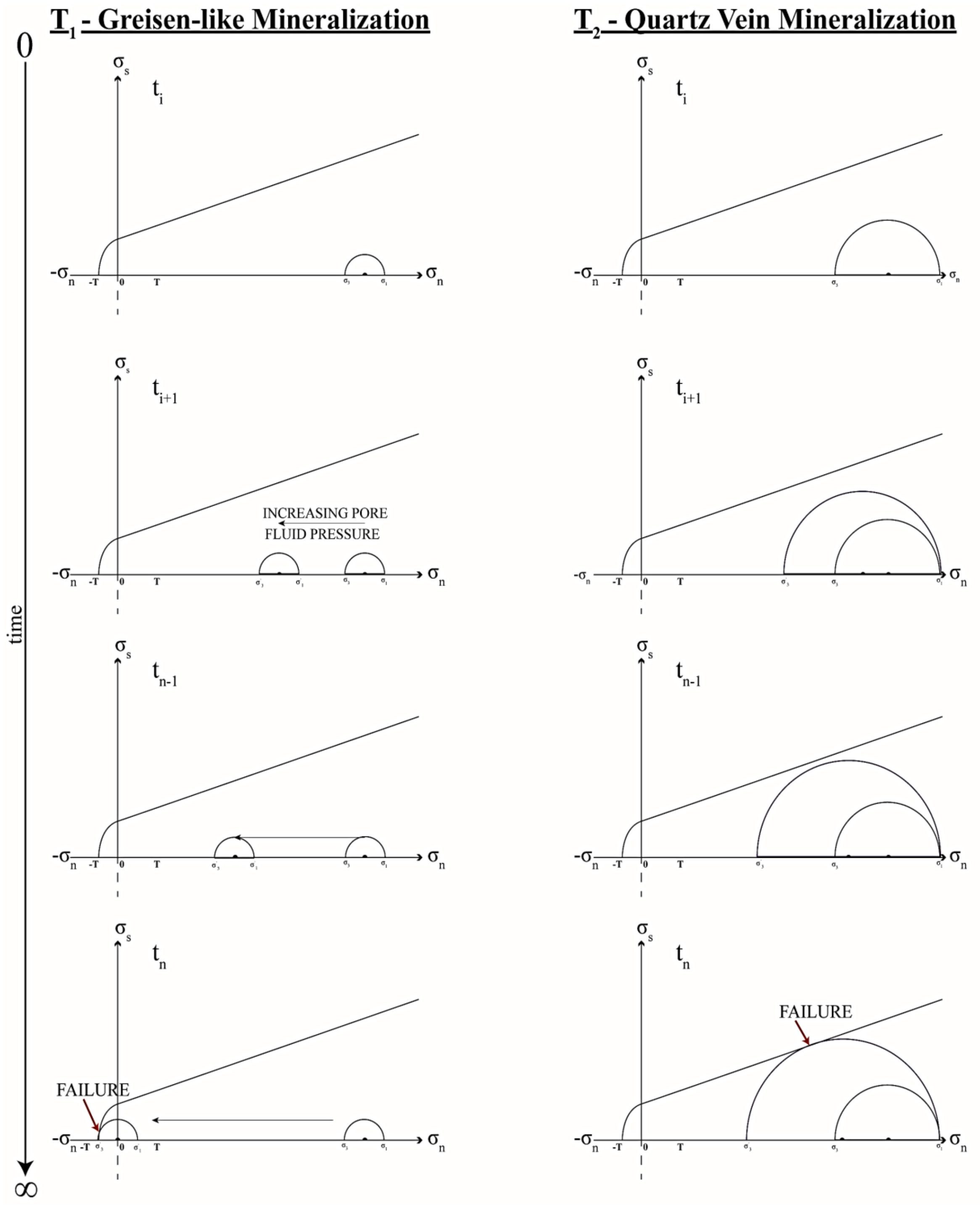

Figure 5.1. The northern sector of the Cacachilas district displays two diverse types of mineralization – greisen-like zones and mineralized quartz veins. This time-progression plot shows potential controls on mineralization for initial greisen-like mineralization (T_1) and the second event, quartz vein mineralization (T_2). Greisen-like alteration was likely controlled by high pore fluid pressure at greater depths; Quartz vein mineralization was likely controlled by increasing differential stresses associated with confining pressure at relatively shallower depths. Both mineralization events are likely seismic-triggered, thus represent a relatively short and cyclic time-scale.

5.3 GENETIC CLASSIFICATION

5.3.1 Epithermal Deposits

Epithermal deposits host precious and base metals, and are mined mainly for gold and silver. Epithermal systems form mostly at shallow crustal levels of less than 1-2 km, or less than 2 km below the water table (Morton, 2009). Epithermal deposits generally form near-surface in mainly island- and continental-arc subduction settings; resultant rock types are subaerial volcanics and calc-alkaline intrusives (Robb, 2005; Morton, 2009). Orebodies are syngenetic to epigenetic of volcanic host rocks and tend to form due to first boiling at depth. Ore deposition extends laterally away from the main source; vein size varies away from source from centimeters to several meters in width. Younger faults may also control mineralization, with remobilization of fluids concentrating the ore. Mineralization takes on many vein forms, including stockwork, stringer, brecciated, and swarms; these vein-types are controlled by pressure-temperature conditions, depth of environment, composition of fluid, acidity of fluid, and gas contents, amongst others (Robb, 2005). Fluid composition and boiling are primary factors that correlate directly to ore deposition.

Epithermal deposits are commonly subdivided into two categories – high-sulfidation or low-sulfidation. This characterization is determined by geologic environment, alteration mineralogy, and fluid chemistry (Cooke & Simmons, 2000). Low-sulfidation systems form proximal to intrusives, where ore deposition is associated with quartz-adularia-sericite-carbonate alteration and occurs generally above the magmatic heat source. The water source for low-sulfidation systems is usually meteoric with magmatic interactions, and fluids tend to be near-neutral pH. Temperatures are less than 300^{o}C.

Conversely, high-sulfidation systems correlate to proximity of degassing calc-alkaline magmas, with ore deposition associated with quartz-alunite-kaolinite-pyrophyllite characteristic alteration (Cooke & Simmons, 2000). Fluid source is mostly magmatic, with minor meteoric interaction and resultant pH is acidic. Temperature ranges from 100°C to greater than 400°C.

5.3.2 Mesothermal Deposits

Mesothermal gold deposits generally form in accretionary regimes with recurring subduction-induced compressive to transpressive deformation. Mesothermal systems form at depths greater than epithermal systems, which is depths greater than 2-6 kilometers (Groves, 1998; Robb, 2005). Active metamorphic and magmatic fluids dominate mesothermal deposits and may likely interact in or near roofs of actively plutonic regions; this fluid interaction locally occurs in the roots of brittle high-angle reverse faults (Sibson, 1988). High-angle reverse faults at great depths promote the fault valve model (discussed earlier), and cyclic-fluctuating fluid pressure causes fracturing once it achieves equal or great values than the lithostatic load. Quartz veins are dominant and have a lower iron sulfide abundance and carbonitic, phyllitic, and/or chloritic alteration overprint. Fluids that mobilize ore are near-neutral and low salinity, transporting gold under reduced sulfur conditions (Groves et al., 1998). Mineralization is structurally controlled, especially at a large-scale; structural controls are ductile to brittle, and are highly variable in size, dip, and displacement (Groves et al., 1998). Brittle-ductile styles of deformation in mesothermal deposits include discrete shears and vein fractures as well as schistose shear-zones (Sibson, 1988). Fluid motion is commonly controlled by pressure fluctuations along pre-existing faults or shear zones, with cyclic formation as movement abruptly accommodates pressure build-up.

5.4 NEARBY DEPOSITS

Historically, extraction of Ag, Au, and Pb along epithermal to mesothermal systems occurred throughout the LCB since the late 1700s. Most operations over this period have been fairly small scale, but deposits continue to be mined and more data on their deposit styles are acquired. Characterization of deposits of the LCB can be classified into three main categories: epithermal vein systems, fault-related disseminated gold, and metamorphic-hosted disseminated gold (Carrillo-Chávez, 1997). Generally, mineralization is related to fault zones, contact zones, and veins. Fluids along these zones commonly exhibit prismatic quartz veins with limonitic alteration, specifically jarosite. Mylonitization occurs within many of the deposits, but is quite variable in both pervasiveness and relation to mineralization. Quartz veinlets and disseminated gold are associated with brittle-ductile shear zones and mylonitic zones.

A general description and classification of proximal deposits are provided here to better contextualize the Cacachilas district at a regional scale. It should be noted that this is not an exhaustive list of deposits on the LCB. Instead, I provide a short synopsis of each deposit to then summarize the similarities, differences, and/or key factors relating specifically to the Cacachilas district.

5.4.1 Los Uvares

The Los Uvares deposit is located in the central portion of the Los Cabos Block (Figure 1.2) and is classified as a disseminated gold epithermal deposit. The deposit is hosted within cataclastically deformed tonalitic Cretaceous rocks which is cut by faults and diorite dikes (Carrillo-Chávez, 1997). Tonalite and diorite within the Los Uvares region have radiometric dates of 137 Ma and 128 Ma, respectively; these intrusive rocks are older than most other intrusive rocks along the LCB. Apatite fission-track ages suggest mineralization dates of about 100 Ma to 80 Ma (Carrillo-Chávez, 1997), thus mineralization of the Los Uvares deposit is similar in age to other deposits located on the LCB. Mineralization occurs in a 12-25 m wide fault zone that strikes generally northwest and dips 50º-65º northeast (Carrillo-Chávez, 1997). Gold is associated with sericite-quartz-pyrite alteration in the brecciated and fractured tonalite and diorite. Higher gold grades are concentrated in the cataclastic tonalite, yet also return high results with less deformed rocks. Gold values decrease in association with calcite, which may be explained by remobilization and/or dilution of gold during a later stage of alteration. Propylitic, kaolinitic, and silicic alteration occurs near mineralized structures with moderate quartz-sericite alteration along mineralized structural features (Bustamente-Garcia, 2000).

5.4.2 Las Colinas/La Colpa/Los Planes

The Las Colinas gold deposit is located 20 km south of the Sierra Cacachilas, approximately 40 km east of La Paz, and approximately 10 km south of El Triunfo (Figure 1.2). Shear zones in the Las Colinas deposit trend north-south, dip generally 45º west, and are approximately 4 to 8 meters in width (Coyan, 2007; Herdrick, 2009). Remnant sedimentary roof pendants of Paleozoic to mid-Mesozoic rocks are products of contact metamorphism and regional ductile deformation. Plutons that uplifted these roof pendants are variable in lithology within the deposit and occur in multiple phases. Oldest plutons are mainly in the southern area of the Colinas area near the La Colpa mine. These plutons range from diorite to gabbro with high percentages of hornblende or augite and are also exposed around Paredones and Uvares (Herdrick, 2009). Next in succession is a biotite-hornblende-quartz-diorite batholith ranging compositionally from gabbro to quartz diorite and granodiorite. This igneous body is east of La Paz and extends southward through Todos Santos (Herdrick, 2009). A hornblende-rich intrusion cuts through the large dioritic igneous body and intrudes into the remnant metasedimentary roof pendants. Foliation is locally developed in the hornblende-rich intrusive, and is cut by pegmatitic and aplitic dikes (Herdrick, 2009).

Three sets of faults define the Los Planes region; large-scale low-angle faults, a high-angle fault, and a strike-slip fault. Large-scale low-angle faults are characterized by cataclasites and mylonites within the stockwork-type mineralized veins. Shear zones in Los Planes and Las Colinas dip approximately 45 degrees to the west (Herdrick, 2009). The high-angle fault trends north and dips subvertical towards the east. The strike-slip fault trends north, passing through the town of San Antonio and possibly continuing northward, west of El Sargento and west of the Cacachilas district along the foothills of the Sierra Cacachilas (Figure 1.2). This strike-slip fault is likely associated with extension and rifting of the Baja California. There exist normal faults that trend northwest and are likely Pleistocene in age (Herdrick, 2009; Busch et al., 2011), but these faults do not appear to control hypogene mineralization. They may be responsible for increasing fluid circulation of groundwater, thereby causing supergene enrichment of the deposit near-surface, or near the water table.

An overprinting sericitic alteration is weakly pervasive south of the Colinas deposit and southeast of La Colpa; this sericitic alteration may also be present in the footwall of Los Planes. Mineralization is stockwork-type, and is localized to cataclasite to mylonite units that run sub-parallel and trend north, (Herdrick, 2009). Fluid pathways that mobilize and concentrate mineralization tend to flow along brittle structures with sulfide abundances up to 20% (Herdrick, 2009; Coyan, 2007).

5.4.3 Paredones Amarillos

The Paredones Amarillos gold deposit lies on the northwest side of the Picacho Sierra la Laguna mountain range (Figure 1.2). Located in a crystalline complex, Paredones Amarillos host rocks include metamorphosed Mesozoic sedimentary rocks that are cut by Cretaceous intermediate to silicic intrusive rocks. The western edge of the prospect is cut by the La Paz fault. The dominant rock type on the property is a dioritic complex, which also includes a 129 Ma gabbro (Kuestermeyer et al., 2008). Foliation has a schistose to gneissic texture that increases in proximity to faults, aplitic dikes and a cataclasite. A relatively unfoliated granodiorite intrusive is dated by K-Ar as approximately 91.3 Ma (same as greisen-like mineralization in the Cacachilas granodiorite pluton) and cuts through the diorite. A low-angle shear zone ranges from 10 to 80 m in thickness, strikes north to north-north-east and dips generally 30^{o} southeast separates diorite and granodiorite at surface, and extends through granodiorite at depth. Post-mineralization andesite and dacite dikes have been dated at approximately 74 Ma, cross-cut mineralization, strike 140°-160°, and dip steeply southwest (same strike as pink and white granite dikes in Cacachilas district).

Most of the gold mineralization is constrained to the cataclastic low-angle shear zone and grades a few meters to tens of meters into the granodiorite (Kuestermeyer et al., 2008). Secondary gold mineralization is located in quartz-sulfide micro-veinlets within the intensely brittle-sheared basal section of the diorite directly above the low-angle zone. Along the fault-induced cataclasite, minor amounts of chlorite and fine-grained quartz alteration exists, but sericite is the dominant product of alteration (Kuestermeyer et al., 2008). Sericitic alteration also overprints igneous bodies and has a radiometric date of ~91.3 Ma (Herdrick, 2009; Wachtor, unpublished), which is ±1 Ma of dated gold mineralization in Los Planes and Las Colinas. No obvious correlation is noted between mineralization and oxidation, although oxidation is sporadically present. Mineralization correlates directly with sulfide abundance; sulfides present include pyrite, arsenopyrite, pyrrhotite, and minor chalcopyrite (Kuestermeyer et al., 2008). Gold mineralization in Paredones is considered similar to a mesothermal deposit, with mineralization related to the low-angle shear zone.

5.4.4 El Triunfo

El Triunfo is a silver-dominated shear-zone deposit hosted within metamorphic and igneous assemblages. Shear zones trend generally 020° and dip 15° to 40° east (Herdrick, 2009). Veins run through both the batholith and country rock and represent shear-zone fabrics within El Triunfo (Bustamante-Garcia, 2000). Radiometric cooling ages of dioritic gneisses using the K-Ar method report an age around 75 Ma, which is relatively younger than batholithic emplacement ages within the El Triunfo District (Bustamente-Garcia, 2000). Intrusive igneous rock assemblages include predominantly granodioritic to granitic with local quartz monzonites, gabbros and aplites (Bustamente-Garcia, 2000). The igneous units host most of the mineralized veins and a portion of the shear zones. Narrow veins within igneous bodies are rich in gold, silver, lead, and zinc sulfides. Dikes within the El Triunfo District are of dioritic to rhyolitic composition and strike between 030^o to 070^o, dip variably to the SE, and range in from 1 – 5 meters in average thickness (Bustamente-Garcia, 2000).

5.5 CLASSIFICATION OF THE CACACHILAS DISTRICT

The Cacachilas district is best characterized as a shear zone-hosted mesothermal deposit with minor epithermal-style features that formed locally along shear zones and faults in subsidiary weakened dilatational jogs, or during continued exhumation of the pluton. Shear zones hosted in the Sierra Cacachilas exemplify mesothermal lode gold systems by several key criteria (Bierlein & Crowe, 2000); they are associated in space and time with a compressional subduction setting, form near or above the brittle-ductile transition zone, are structurally controlled, exhibit hydrothermal magmatic and/or metamorphic devolatilization fluid reactions, are vertically constrained, and demonstrate alteration-induced silicification, sericitization, chloritization, albitization and/or sulfidation overprints. All of these features have been observed or documented for the Cacachilas district. Furthermore, regional metamorphism of the Baja up to amphibolite facies also suggests potential for a mesothermal-style system.

Sources of mineralizing fluids are currently unknown, but sericitic alteration is likely associated with metamorphic and/or magmatic fluids at greater depths, whereas quartz veins are likely associated with magmatic hydrothermal and minor meteoric fluids at relatively shallower depths as a result of exhumation and cooling of the pluton. Several key pieces of evidence indicate that magmatic fluids play a large role in alteration along shear zones within the Cacachilas district. Age of the greisen-like zones is 92.4 Ma (Wachtor, unpublished), which coincides with 92.1 Ma radiometric ages of sericitic alteration at Paredones Amarillos (Herdrick, 2009), and regional subduction and related plutonism. Furthermore, potassium alteration is the overarching chemical control on mineralization; potassium prefers to stay in the melt, thus it is commonly the last element along with silica to crystallize out of the melt. Ergo, it is likely that greisen-like zones, and quartz veins were emplaced during the last gasps of pluton emplacement, cooling, and uplift. At late stages of pluton crystallization, as felsic magma becomes water-saturated, the exsolution of aqueous fluid forms quartz veins from the remaining silicate melt. Also known as vapor-saturation or "first boiling," this process is accomplished either by progressive crystallization of the magma, or more likely, by decreasing pressure of the system (Morton, 2009) associated with uplift.

Relative to other deposits located throughout the LCB, the lack of mylonites and abundance of brittle to brittle-ductile quartz vein shear zones within the Cacachilas district might indicate shallower formation depths, but mylonitic rocks in some of these deposits clearly predate late-brittle controlled mineralization (Stephen Reynolds, personal communication). Plutonic and mafic rocks located in Baja are temporally and petrologically associated, and range from felsic to mafic in composition and approximately 140 MA to 90 Ma in age (Fletcher, 2000; Schaaf, 2000; Kimbrough et al., 2014). Most shear zones within the felsic- and mafic-dominated deposits located on the LCB trend N to NE, except for the Los Uvares deposit where mineralized faults trends NW. Mineralization is mostly Cretaceous in age (circa 90-80 Ma) for previously mentioned deposits along the Baja, but is poorly constrained at Las Colinas.

Perhaps subsidiary mineralized structures between major breaks, otherwise known as fault jogs, explain sub-parallel quartz veins to the overall trend of mineralized zones. An en- echelon style emplacement method of mineralized veins seems difficult to achieve. However, to best understand emplacement style of quartz veins, fluid inclusions and radiometric ages are ideal; fluid inclusions will better identify and constrain fluid types moving through the system, and radiometric ages would confirm that quartz vein emplacement did indeed form contemporaneous to greisen-like pods. Orientation of the quartz veins is slightly more constrained than greisen-like pods which is a result of 1) lower fluid pressure associated with uplift and cooling of the pluton, thus rocks cannot fracture as easily and are thereby constrained to break along weaker principle stress planes, or 2) the number of strikes and trends measured (n-factor) for greisen-like pods is too low and thus not an acceptable representation of true greisen-like trends.

A comparison of mainland Mexico deposits may shed light on tectonic history of the LCB, and/or may help to better constrain future exploration of deposits associated with pluton-hosted shear zones. Furthermore, a comparison to similar style shear zone-hosted deposits within an igneous pluton may shed further light on emplacement mechanisms of mineralization. Similar style deposits include Mother Lode, Coeur d'Alene, Yellowknife, Vulture Mine, and La Herradura.

6. CONCLUSION

Unexplored since the early 1900s, the Cacachilas district was long forgotten until recent ventures to explore and re-assess the deposit. Further exploration work is still needed to understand the full extent of the deposits in the Sierra Cacachilas. A combination of geophysical and exploration mapping of the deposits has shed new insights on the nature and distribution of the deposits and their economic viability. After extensive field work and literature review, mineralization is best classified as shear-zone-hosted gold and silver, mesothermal-style deposits hosted entirely within a granodiorite-tonalite pluton. Although there is significantly less ductile deformation and consequent mineralization, this characterization is similar to other deposits throughout the LCB.

Two main events of mineralization are differentiable within the pluton. First is emplacement of greisen-like pods and the second is quartz-vein mineralization. Greisen-like vein-like and podiform structures form under a ductile to brittle regime at greater depths and pressures. Mineralized quartz veins form later, probably during the exhumation and cooling process of the pluton under a brittle to brittle-ductile regime at relatively shallower depths and pressures. Sericitic alteration dominates the first mineralizing event, while silicic, sericitic, and potassic alteration dominate the second mineralizing event. This further indicates that both events likely formed during emplacement and cooling of the pluton at 92.4 Ma (Wachtor, unpublished) associated with regional subduction and plutonism.

Mineralization within the northern Cacachilas district mainly trends NE, varies in dip from 30^{o}-88^{o}, and crosscuts the pluton and associated dikes. Orientation does not change between mineralization events, indicating a similar orientation of the weakest principle stress (σ_3). However, pink and white aplitic granite dikes have an emplacement age older than either mineralization event and have a different orientation, thus indicating that during or after emplacement of the pluton, there was a change in the orientation of principle stresses.

Alteration plays a significant role within the district. Limonitic alteration may indicate and help locate higher grade ore. Potassic and sericitic alteration overprint is also evident along shear zones and may prove significant for identifying mineralized zones. Results from assays indicate there may be some type of hydrothermal, magmatic, or metamorphic fluid alteration that trends west to east within the district. Alteration that correlates to economic grades along the shear zones include: breakdown of biotite and potassium feldspar into sericite; potassic alteration evidenced by secondary potassium feldspar, and sericitic +/- chloritic alteration along greisen-like zones; and silicic and potassic alteration evidenced by breakdown of the country rock surrounding quartz veins via secondary potassium feldspar, and kaolinite alteration along with open space, prismatic quartz and subhedral to euhedral sulfides. Overall, base metal values increase from east to west, but further geochemical analysis, reflected light microscopy, and fluid inclusion[1] analyses are needed to shed light on the overall geochemistry of the pluton to determine whether these trends are associated with pluton emplacement or hydrothermal, magmatic,

[1] Fluid inclusion samples were collected in the field and sent out to AZ Quality Thin sections for 100-micron polished thin sections. Fluid inclusion analysis will be supplemental work done at Tucson's USGS office by ASU colleague Megan Miller at a future time.

or metamorphic fluids. Furthermore, these analyses may determine what the gold and silver are associated with (pyrite, arsenopyrite, or other) at the micron-scale.

Historic trends within the northern section of the Cacachilas district that prove promising targets and best exemplify higher grades associated with the above-mentioned mineralization and alteration characteristics include the La Casualidad/Santa Teresa, La Libertad, and Animas trends. Trends that may yet prove economic, but require in-depth geochemical analyses along the entire trend include Pisos and El Tesoro. Finally, trends that returned low gold and silver values relative to other mineralized trends within the northern sector and rest of the district, but may yet prove economic include Matancitas, and the newly discovered north trending prospect, tentatively named the Don Victor Prospect. If prefeasibility planning and production do eventually begin within the district, the higher grade trends within the northern sector (La Casualidad/Santa Teresa, La Libertad and Animas) as well as higher grade trends located south of my field area (i.e., Wachtor thesis, unpublished) should be developed first. Secondary focus of the lesser grade trends (Pisos and El Tesoro) should occur after the initial planning and metal extraction phases are initiated. It should be noted that secondary targets still require extensive analysis and combination of geophysical and geological data. Furthermore, due to the variability of mineralization abundance along each trend, I suggest that a surficial geochemical analysis be carried out to better determine base and precious metal location and abundance. A synthesis of geological, geophysical, geochemical, and drill core data is necessary to best characterize individual shear zones along trend and at depth and to understand the extent and economic viability of the Cacachilas district.

REFERENCES

Alsleben, H., Wetmore, P.H., Gehrels, G.E., and Paterson, S. R. (2012). Detrital zircon ages in Palaeozoic and Mesozoic basement assemblages of the Peninsular Ranges batholith, Baja California, Mexico: constraints for depositional ages and provenance. *International Geology Review*, *54*(1), 93–110.

Atwater, T. (1970). Implications of plate tectonics for the Cenozoic evolution of western North America. *Geological Society of America*, 81, 3513-3536.

Bierlein, F.P., and Crowe, D.E. (2000). Phanerozoic orogenic lode gold deposits. *Reviews in Economic Geology*, 13, 130-40.

Busby, C. (2004). Continental growth at convergent margins facing large ocean basins: a case study from Mesozoic convergent-margin basins of Baja California, Mexico. *Tectonophysics*, *392*(1-4), 241–277. http://doi.org/10.1016/j.tecto.2004.04.017

Busby, C., Smith, D., Morris, W., & Fackler-Adams, B. (1998). Evolutionary model for convergent margins facing large ocean basins: Mesozoic Baja California, Mexico. *Geology*, *26*(3), 227–230.

Busch, M. M., Arrowsmith, J. R., Umhoefer, P. J., Coyan, J. A., Maloney, S. J., & Gutierrez, G. M. (2011). Geometry and evolution of rift-margin, normal-fault-bounded basins from gravity and geology, La Paz-Los Cabos region, Baja California Sur, Mexico. *Lithosphere*, *3*(2), 110–127. http://doi.org/10.1130/L113.1

Bustamante-Garcia, J. (2000). Geology Mining Monograph of the State of Baja California Sur, Consejo Recursos Minerales Monograph M 24, 232 pp., 3 plates.

Carrillo, A., & Huyck, H. (1997). A genetic model for the Los Uvares gold deposit, Baja California Sur, Mexico, *36*. Universidad Nacional Autonoma de Mexico. ISSN: 0016-7169.

Carrillo-Chavez, A., Huyck, H., Zentilli, M., & Griest, A. (1999). Age constraints on host rocks of Los Uvares gold deposit : Magmatic pulses in southernmost Baja California, Mexico. *Geofisica Internacional*, *38*(1), 27–33.

Coyan, J. (2007). The Structural Setting of Hydrothermal Gold Deposits in the San Antonio Area, Baja California Sur, Mexico. PhD dissertation, Arizona State University.

Dickinson, W. R., & Lawton, T. F. (2001). Carboniferous to Cretaceous assembly and fragmentation of Mexico. *Geological Society of America Bulletin*, *113*(2000), 1142–1160.

Dixon, T., Farina, F., DeMets, C., Suarez-Vidal, F., Fletcher, J., Marquez-Azua, B., Umhoefer, P. (2000). New Kinematic Models for Pacific-North America Motion from 3 Ma to Present, II: Evidence for a "Baja California shear zone." *Geophysical Research Letters*, *27*(23), 3961–3964.

Fletcher, J. M., Grove, M., Kimbrough, D., Lovera, O., & Gehrels, G. E. (2007). Ridge-trench interactions and the Neogene tectonic evolution of the Magdalena shelf and southern Gulf of California: Insights from detrital zircon U-Pb ages from the Magdalena fan and adjacent areas. *Geological Society of America Bulletin*, *119*(11-12), 1313–1336. http://doi.org/10.1130/B26067.1

Fletcher, J. M., Kohn, B. P., Foster, D. A., Gleadow, A. J. W., Fletcher, J. M. (2000). Heterogeneous Neogene cooling and exhumation of the Los Cabos block, southern Baja California: Evidence from fission-track thermochronology. *Geology*, *28*(2), 107–110. http://doi.org/10.1130/0091-7613(2000)28<107

Fletcher, J. M., & Munguia, L. (2000). Active continental rifting in southern Baja California, Mexico: Implications for plate motion partitioning and the transition to seafloor spreading in the Gulf of California. *Tectonics*, *19*(6), 1107–1123.

Goldfarb, R. J., Groves, D. I., & Gardoll, S. (2001). Orogenic gold and geologic time: a global synthesis. *Ore Geology Reviews, 18*, 1–75.

Groves, D. ., Goldfarb, R. ., Gebre-Mariam, M., Hagemann, S. ., & Robert, F. (1998). Orogenic gold deposits: A proposed classification in the context of their crustal distribution and relationship to other gold deposit types. *Ore Geology Reviews*, *13*(1-5), 7–27. http://doi.org/10.1016/S0169-1368(97)00012-7

Hausback, B. P. (1984). Cenozoic volcanic and tectonic evolution of Baja California Sur, Mexico. *Pacific Section S.E.P.M.1*, *39*, 219–236.

Herdrick, M. A., and Giroux, G. H. (2009). Technical report and resource update, San Antonio Gold Project, Baja California Sur. *Pediment Gold Corp*.

Kimbrough, D. L., Grove, M., & Morton, D. M. (2014). Timing and significance of gabbro emplacement within two distinct plutonic domains of the Peninsular Ranges batholith, southern and Baja California. *Geological Society of America Bulletin*, (July). http://doi.org/10.1130/B30914.1

Kuestermeyer, A., Ramirez, D., Bentzen, E., Earnest, F., Pablo Dorantes, J.E., Deter, K., Michael, N., and Mandziak, T. (2008). Feasibility Study NI 43-101 Technical Report; Paredones Amarilos Gold Project, Baja Californa Sur, Mexico. *Vista Gold Corp*.

Morton, R. (2009). A Brief Guide to the Geology of Ore Deposits. University of Minnesota Duluth, Economic Geology – GLG4350.

Orynski, L. (1889). The Cacachilas District; Gold and Silver Mining Co., of Lower California, Mexico. Publisher unknown.

Padilla y Sanchez, R. (2013). Tectonic Map of Mexico database. Division de Ingenieria en Ciencias de la Tierra, Facultad de Ingenieria, Universidad Nacional Autonoma de Mexico (UNAM).

Robb, L. (2005). Introduction to Ore-Forming Processes. *Blackwell Publishing, Wiley*.

Schaaf, P., Bohnel, H., & Perez-Venzor, J. A. (2000). Pre-Miocene palaeogeography of the Los Cabos Block, Baja California Sur: geochronological and palaeomagnetic constraints. *Tectonophysics*, *318*, 53–69.

Sedlock, R.L. (2003). Geology and tectonics of the Baja California peninsula and adjacent areas, *Geological Society of America Special Paper*, 374, 1 - 42.

Sibson, R. H., Moore, J. M., and Rankin, A. H. (1975). Seismic pumping: a hydrothermal fluid transport mechanism. *Journal of the Geological Society London*, 131, 653-9.

Sibson, R.H., Robert, F., and Poulsen, K.H. (1988). High-angle reverse faults, fluid-pressure cycling, and mesothermal gold-quartz deposits, *Geology*, 16 (6), 551 – 555, doi:10.1130/0091-7613(1988)016.

Sibson, R. H. (1994). Crustal stress, faulting and fluid flow. In J. Parnell (ed.), Geofluids: Origin, Migration and Evolution of Fluids in Sedimentary Basins. *Geological Society, Special Publication*, *78*, 69-84.

Sibson, R. H., & Scott, J. (1998). Stress/fault controls on the containment and release of overpressured fluids: Examples from gold-quartz vein systems in Juneau, Alaska; Victoria, Australia and Otago, New Zealand. *Ore Geology Reviews*, *13*, 293–306.

Smith, W. H. F., and Sandwell, D. T. (1997). Global seafloor topography from satellite altimetry and ship depth soundings. *Science*, v. 277, 1957-1962.

Stock, J. M., & Hodges, K. V. (1989). Pre-Pliocene extension around the Gulf of California and the transfer of Baja California to the Pacific Plate. *Tectonics*, *8*(1), 99–115.

Wachtor, S. (unpublished). Shear-zone hosted mineralization in the Sierra Cacachilas, Baja California Sur, Mexico. M.Sc. Thesis, Arizona State University.

Withjack, M.O., and Jamison, W.R. (1986). Deformation produced by oblique rifting. *Tectonophysics*, v. 126, 99–124, doi:10.1016/0040-1951(86)90222-2.

APPENDIX A

COLLECTED FIELD DATA

GIS Code Key

0 = granodiorite	4 = pink granite dike
1 = quartz vein	5 = white granite dike
2 = greisen-like zone	6 = fault gauge
3 = mineralized zone	7 = other/mojanera

ID	Easting	Northing	GIS Code	Limonite [2] Intensity (0-4)	Type of Measure-ment[3]	Strike/ Trend	Dip/ Plunge	Sample (0=no sample; 1=sample)
BCARS-001	596026	2669608	0	-	S/D	120	65	0
BCARS-002	-	-	1	-	S/D	30	86	0
BCARS-003	596051	2669569	0	0	-	-	-	0
BCARS-004	596052	2669594	0	1	S/D	150	80	0
BCARS-005	596026	2669608	0	1	S/D	104	60	0
BCARS-005	596026	2669608	0	1	S/D	90	50	0
BCARS-005	596026	2669608	0	1	S/D	104	58	0
BCARS-005	596026	2669608	0	1	S/D	102	85	0
BCARS-005	596026	2669608	0	1	S/D	357	80	0
BCARS-005	596026	2669608	0	1	S/D	46	85	0
BCARS-005	596026	2669608	0	1	S/D	48	65	0
BCARS-005	596026	2669608	0	1	S/D	45	80	0
BCARS-005	596026	2669608	0	1	T/P	-	10	0
BCARS-006	596022	2669596	0	0	-	-	-	0
BCARS-007	596021	2669588	1	3	Trend	22	-	1
BCARS-007	596021	2669588	1	3	Trend	17	-	1
BCARS-008	596026	2669563	8	2	-	-	-	0
BCARS-009	596019	2669561	3	2	-	-	-	0
BCARS-010	596010	2669544	0	1	S/D	130	85	0

[2] Limonite intensity scale ratings: 0 = none, 1 = weak, 2 = moderate, 3 = strong, 4 = pervasive
[3] S/D = strike/dip, T/P = trend/plunge

BCARS-010	596010	2669544	0	1	Trend	20	-	0
BCARS-011	596004	2669526	4	0	-	-	-	0
BCARS-012	595996	2669515	3	-	-	-	-	0
BCARS-013	595982	2669486	0	1	-	-	-	0
BCARS-014	595987	2669468	1	2	-	-	-	1
BCARS-015	596018	2669631	1	1	-	-	-	0
BCARS-016	596027	2669661	3	3	-	-	-	0
BCARS-017	596075	2669619	0	1	-	-	-	0
BCARS-018	596047	2669685	0	0	-	-	-	0
BCARS-019	596031	2669697	1	2	-	-	-	0
BCARS-020	596040	2669718	1	3	S/D	20	-	0
BCARS-021	596054	2669713	0	0	-	-	-	0
MT-017	596078	2669768	0	0	-	-	-	0
BCARS-022	596045	2669767	1	2	Trend	70	-	0
BCARS-022	596045	2669767	1	2	Trend	20	-	0
BCARS-023a	596050	2669794	1	1	-	-	-	0
BCARS-023b	596044	2669803	0	0	-	-	-	0
MT-021	596027	2669810	0	0	-	-	-	0
MT-022	595962	2668807	0	-	-	-	-	0
BCARS-024	596016	2669822	0	0	-	-	-	0
BCARS-025	595747	2669602	0	0	-	-	-	0
BCARS-026	595608	2669618	4	0	Trend	315	-	0
BCARS-027	595402	2669539	2	3	-	-	-	0
BCARS-028	595400	2669507	2	2	-	-	-	0
BCARS-029	595221	2669364	2	4	-	-	-	1
BCARS-030	594870	2669035	0	0	-	-	-	0
BCARS-031	594898	2669066	2	2	-	-	-	0
BCARS-032	594912	2669103	0	0	-	-	-	0

BCARS-033	594965	2669086	2	3	-	-	-	1
BCARS-034	594995	2669109	2	2	Trend	65	-	0
BCARS-035	595017	2669138	2	4	Trend	65	-	0
BCARS-036	595026	2669167	2	2	-	-	-	0
BCARS-037	595025	2669177	0	0	-	-	-	0
BCARS-038A	594991	2669159	3	4	Trend	24	-	0
BCARS-038	595000	269175	3	4	-	-	-	0
BCARS-039	595003	2669208	2	-	-	-	-	0
BCARS-040	595035	2669245	2	2	-	-	-	0
BCARS-041	595059	2669258	2	2	Trend	57	-	0
BCARS-042	595048	2669277	2	3	-	-	-	0
BCARS-043	595057	2669303	2	-	Trend	18	-	0
BCARS-044	595090	2669271	2	-	-	-	-	0
BCARS-045	595156	2669290	6	2	S/D	40	50	0
BCARS-046	595144	2669299	0	4	-	-	-	0
BCARS-047	595159	2669366	0	0	-	-	-	0
BCARS-048	595121	2669330	0	0	Trend	65	-	0
BCARS-048	595121	2669330	0	0	Trend	305	-	0
BCARS-049	595195	2669258	2	-	-	-	-	0
BCARS-050	595213	2669372	2	2	-	-	-	1
BCARS-051	595210	2669418	2	2	-	-	-	0
BCARS-052	595216	2669443	2	-	-	-	-	0
BCARS-053	595249	2669325	2	-	-	-	-	0
BCARS-054	595224	2669282	2	2	S/D	44	48	0
BCARS-055	595215	2669276	2	2	-	-	-	0
BCARS-056	595213	2669372	2	-	-	-	-	0

BCARS-057	595199	2669453	2	2	-	-	-	0
BCARS-058	595199	2669469	0	-	-	-	-	0
BCARS-059	595248	2669372	2	3	Trend	30	-	0
BCARS-060	595243	2669360	2	-	-	-	-	0
BCARS-061	595254	2669382	2	-	Trend	10	-	0
BCARS-062	595269	2669390	0	0	-	-	-	0
BCARS-063	595259	2669404	2	-	-	-	-	0
BCARS-064	595291	2669472	7	0	-	-	-	0
BCARS-065	595249	2669502	7	0	-	-	-	0
BCARS-066	595274	2669281	0	0	-	-	-	0
BCARS-067	595307	2669231	2	4	Trend	25	-	1
BCARS-068	595285	2669206	2	-	-	-	-	0
BCARS-069	595211	2669276	2	-	Trend	52	-	0
BCARS-070	595086	2669286	0	0	-	-	-	0
BCARS-071	595103	2669298	2	-	Trend	180	-	0
BCARS-072	595023	2669282	2	-	Trend	70	-	0
BCARS-073	594998	2669278	2	-	-	-	-	0
BCARS-074	594987	2669142	2	-	Trend	70	-	0
BCARS-075	596592	2665333	3	-	S/D	0	76	1
BCARS-076	595194	2668369	3	-	-	-	-	0
BCARS-077	595321	2668331	5	1	Trend	85	-	0
BCARS-078	595408	2668323	1	3	S/D	40	60	1
BCARS-078	595408	2668323	1	3	S/D	45	80	1
BCARS-078	595408	2668323	1	3	S/D	90	60	1
BCARS-078	595408	2668323	1	3	S/D	20	75	1
BCARS-079	595463	2668321	1	2	S/D	50	87	0

BCARS-080	595578	2668350	1	2	S/D	270	60	0
BCARS-081	595585	2668362	1	-	Trend	295	-	0
BCARS-082	595609	2668406	3	3	Trend	6	-	0
BCARS-083	595641	2668383	3	2	-	-	-	0
BCARS-084	595793	2668562	0	0	-	-	-	0
BCARS-085	595847	2668732	1	2	Trend	90	-	0
BCARS-085	595847	2668732	1	2	Trend	218	-	0
BCARS-085	595847	2668732	1	2	Trend	200	-	0
BCARS-086	595832	2668763	0	0	-	-	-	0
BCARS-087	595792	2668789	1	2	S/D	126	82	0
BCARS-088	595860	2669292	0	0	-	-	-	0
BCARS-089	595909	2669393	0	0	-	-	-	0
BCARS-090	595941	2669380	1	0	S/D	25	45	0
BCARS-091	596032	2669358	0	0	-	-	-	0
BCARS-092	596030	2669380	4	0	-	-	-	0
BCARS-093	596045	2669415	6	-	-	-	-	1
BCARS-094	595913	2669340	4	-	Trend	330	-	0
BCARS-095	595876	2669386	4	-	Trend	290	-	0
BCARS-096	595951	2669357	1	2	Trend	20	-	0
BCARS-097	595947	2669322	3	2	Trend	20	-	1
BCARS-098	595042	2668121	0	0	-	-	-	0
BCARS-099	595020	2668092	1	1	S/D	68	70	0
BCARS-100	594969	2668112	0	-	-	-	-	0
BCARS-101	594900	2668126	0	-	-	-	-	0
BCARS-102	594904	2668139	1	1	-	-	-	0
BCARS-103	594918	2668147	1	-	S/D	44	40	1

BCARS-104	594897	2668134	1	2	S/D	50	40	1
BCARS-105	594873	2668113	1	4	-	-	-	0
BCARS-106	594865	2668097	1	2	S/D	62	74	0
BCARS-107	594842	2668078	1	-	S/D	42	80	1
BCARS-108	594816	2668059	1	2	S/D	45	65	0
BCARS-109	594904	2668106	2	4	-	-	-	1
BCARS-110	594976	2668138	0	0	-	-	-	0
BCARS-111	594831	2668060	0	1	Trend	70	-	0
BCARS-112	594820	2668046	0	0	S/D	330	90	0
BCARS-113	594813	2668057	1	2	Trend	50	-	0
BCARS-114	594797	2668045	1	2	S/D	62	65	0
BCARS-115	594785	2668036	1	3	S/D	63	70	0
BCARS-115	594785	2668036	1	3	S/D	35	56	0
BCARS-115	594785	2668036	1	3	Trend	90	-	0
BCARS-116	594773	2668020	1	4	Trend	62	-	1
BCARS-117	594751	2667995	1	3	S/D	40	70	0
BCARS-118	594741	2667982	1	3	Trend	62	-	0
BCARS-119	594717	2667965	1	3	S/D	62	72	1
BCARS-120	594688	2667987	0	-	Trend	20	-	0
BCARS-120	594688	2667987	0	-	Trend	336	-	0
BCARS-121	594704	2667950	1	3	Trend	58	-	1
BCARS-122	594676	2667903	1	-	Trend	40	-	0
BCARS-123	594656	2667884	1	-	S/D	42	64	0
BCARS-124	594644	2667866	1	-	S/D	30	70	0
BCARS-125	594625	2667843	4	-	Trend	338	-	0
BCARS-126	594612	2667825	4	-	Trend	308	-	0

BCARS-127	594636	2667801	0	2	-	-	-	0
BCARS-128	594663	2667829	1	2	-	-	-	0
BCARS-129	594659	2667798	1	2	Trend	64	-	1
BCARS-130	594645	2667849	1	2	-	-	-	0
BCARS-131	594656	2667875	1	2	Trend	48	-	0
BCARS-132	594660	2667880	8	-	-	-	-	1
BCARS-133	594663	2667883	1	-	Trend	62	-	0
BCARS-134	594667	2667888	1	-	S/D	42	25	0
BCARS-135	594670	2667895	1	3	-	-	-	0
BCARS-136	594637	2667842	3	2	Trend	66	-	0
BCARS-137	594652	2667737	2	4	-	-	-	0
BCARS-138	594817	2668310	1	2	S/D	56	64	0
BCARS-139	594799	2668285	1	2	S/D	52	58	0
BCARS-140	594753	2668230	1	3	Trend	62	-	0
BCARS-141	594746	2668215	1	2	Trend	58	-	0
BCARS-142	594738	2668161	1	-	Trend	58	-	0
BCARS-143	594709	2668168	3	-	Trend	58	-	0
BCARS-144	594698	2668138	1	3	S/D	58	68	0
BCARS-145	594663	2668135	0	0	-	-	-	0
BCARS-146	594660	2668100	1	-	S/D	70	55	0
BCARS-146	594660	2668100	4	-	S/D	334	80	1
BCARS-147	594628	2668056	0	-	-	-	-	0
BCARS-148	594706	2668150	1	-	Trend	46	-	0
BCARS-149	594694	2668130	1	3	Trend	64	-	0
BCARS-150	594614	2668028	1	2	Trend	50	-	0
BCARS-151	594608	2668022	1	4	S/D	50	70	1

BCARS-151	594608	2668022	5	0	S/D	180	84	1
BCARS-151	594608	2668022	5	0	S/D	160	80	1
BCARS-152	594580	2667983	0	0	-	-	-	0
BCARS-153	594590	2668001	5	0	Trend	330	-	0
BCARS-154	594575	2667970	3	1	Trend	52	-	0
BCARS-155	-	-	5	-	Trend	20	-	0
BCARS-155	-	-	5	-	Trend	60	-	0
BCARS-156	594549	2667987	0	1	S/D	58	64	0
BCARS-156	594549	2667987	0	1	S/D	120	78	0
BCARS-156	594549	2667987	5	1	S/D	154	74	0
BCARS-156	594549	2667987	5	1	S/D	170	87	0
BCARS-157	594561	2668031	0	0	S/D	174	88	0
BCARS-157	594561	2668031	0	0	S/D	172	52	0
BCARS-157	594561	2668031	0	0	S/D	160	64	0
BCARS-158	594578	2668046	0	0	S/D	170	78	0
BCARS-159	594611	2668109	0	0	S/D	44	30	0
BCARS-160	594644	2668116	0	0	-	-	-	0
BCARS-161	594691	2668114	8	-	-	-	-	0
BCARS-162	594684	2668143	1	2	Trend	57	-	0
BCARS-163	-	-	1	0	Trend	74	-	0
BCARS-164	594738	2668183	0	0	-	-	-	0
BCARS-165	595019	2668275	1	2	Trend	6	-	0
BCARS-166	595038	2668365	1	-	-	-	-	0
BCARS-166	595038	2668365	6	-	Trend	63	-	0
BCARS-167	595015	2668337	1	3	Trend	53	-	0
BCARS-168	595008	2668327	1	-	-	-	-	0

BCARS-169	595002	2668320	1	-	S/D	50	74	0
BCARS-170	594870	2667733	1	-	S/D	40	70	0
BCARS-171	594862	2667725	1	2	S/D	38	72	0
BCARS-172	594837	2667707	0	0	-	-	-	0
BCARS-172	594837	2667707	5	-	Trend	154	-	0
BCARS-173	594826	2667686	0	0	Trend	150	-	0
BCARS-174	-	-	2	1	-	-	-	0
BCARS-175	594792	2667679	0	0	-	-	-	0
BCARS-175	594792	2667679	5	0	Trend	166	-	0
BCARS-176	594793	2667661	1	3	Trend	40	-	0
BCARS-177	594774	2667645	4	-	Trend	144	-	0
BCARS-178	594763	2667636	4	-	Trend	32	-	1
BCARS-179	594759	2667630	0	0	-	-	-	0
BCARS-180	594764	2667686	1	2	Trend	32	-	0
BCARS-181	594824	2668345	1	3	Trend	20	-	0
BCARS-182	594822	2668369	3	1	Trend	45	-	0
BCARS-182	594822	2668369	3	1	T/P	34	31	0
BCARS-182	594822	2668369	3	1	S/D	100	50	0
BCARS-182	594822	2668369	3	1	S/D	76	82	0
BCARS-182	594822	2668369	3	1	S/D	97	77	0
BCARS-182	594822	2668369	3	1	S/D	112	82	0
BCARS-183	594858	2668378	0	0	-	-	-	0
BCARS-184	594867	2668383	1	3	S/D	84	62	0
BCARS-185	594848	2668478	0	0	-	-	-	0
BCARS-186	594932	2668473	0	0	-	-	-	0
BCARS-187	594911	2668440	0	0	-	-	-	0

BCARS-188	594918	2668448	4	0	Trend	172	-	0
BCARS-189	594945	2668436	1	4	Trend	18	-	0
BCARS-190	594997	2668409	1	4	-	-	-	1
BCARS-191	595023	2668413	1	4	Trend	72	-	0
BCARS-192	595029	2668376	0	1	Trend	54	-	0
BCARS-193	595026	2668355	1	4	Trend	74	-	0
BCARS-194	595016	2668345	6	-	-	-	-	0
BCARS-195	595017	2668357	6	-	T/P	280	12	0
BCARS-196	595070	2668353	1	0	Trend	30	-	0
BCARS-197	595048	2668334	6	-	-	-	-	0
BCARS-198	595059	2668317	3	1	S/D	45	75	0
BCARS-199	595109	2668322	3	1	Trend	132	-	0
BCARS-200	595099	2668368	6	2	Trend	308	-	0
BCARS-201	595166	2668326	4	0	S/D	30	60	0
BCARS-202	595163	2668367	6	1	-	-	-	0
BCARS-203	595228	2668382	5	0	Trend	348	-	0
BCARS-204	595712	2668404	0	0	-	-	-	0
BCARS-205	595789	2668493	1	2	Trend	328	-	0
BCARS-206	595893	2668484	1	4	S/D	43	20	1
BCARS-207	595838	2668496	1	0	-	-	-	0
BCARS-208	595782	2668882	1	0	-	-	-	0
BCARS-209	595748	26689184	1	0	-	-	-	0
BCARS-210	595857	2669323	5	-	Trend	33o2	-	0
BCARS-211	595940	2669305	1	0	Trend	20	-	0
BCARS-212	595939	2669283	4	-	-	-	-	0
BCARS-213	595927	2669216	0	0	-	-	-	0

BCARS-214	595939	2669174	0	0	Trend	316	-	0
BCARS-215	595903	2669170	1	0	Trend	86	-	0
BCARS-216	595946	2669094	0	-	-	-	-	1
BCARS-217	595360	2668345	0	0	-	-	-	0
OLT-001	595822	2664266		-	-	-	-	0
OLT-002	-	-		-	-	-	-	0
OLT-003	-	-		-	-	-	-	0
Pt-010	-	-		-	-	-	-	0
Pt-011	-	-		-	-	-	-	0
Pt-012	-	-		-	-	-	-	0
Pr-013	-	-		-	-	-	-	0
Chav-001	594856	2660230	2	-	Trend	19	-	1
Chav-002	594383	2659705	2	3	Trend	23	-	0
Chav-003	594357	2659652	0	-	-	-	-	0
1404-001	584184	2671386		-	-	-	-	0
1404-002	584816	2671146		-	-	-	-	0
1404-003	584377	2671968		-	-	-	-	0
1404-004	584351	2671810		-	-	-	-	0
1404-005	583544	2672780		-	-	-	-	0
1404-006	583400	2672780		-	-	-	-	0
1404-007	583720	2672209		-	-	-	-	0
1404-008	583720	2672207		-	-	-	-	0
Chav-004	594826	2660394	3	2	Trend	344	-	0
Chav-005	594739	2660406	3	3	Trend	22	-	0
Chav-006	594585	2660310	0	1	-	-	-	0
Chav-007	594527	2660431	4	-	Trend	37	-	0
Chav-007	594527	2660431	1	-	Trend	330	-	0
Chav-008	594459	2660538	1	4	Trend	346	-	0

Chav-009	594437	2660593	1	-	Trend	350	-	0
Chav-010	594440	2660679	1	4	S/D	26	72	1
Chav-011	594423	2660707	3	3	S/D	14	72	0
Chav-012	594288	2660802	0	-	Trend	341	-	0
Chav-013	594242	2660746	2	3	-	-	-	0
Chav-014	594223	2660792	1	0	Trend	340	-	0
Chav-015	594159	2660807	2	2	S/D	212	82	0
Chav-016	594160	2660783	1	2	-	-	-	0
Chav-017	594262	2660713	2	2	Trend	215	-	0
Chav-018	594274	2660681	2	1	Trend	201	-	0
Chav-019	594263	2660630	0	0	-	-	-	0
Chav-020	594225	2660628	0	1	Trend	285	-	0
Chav-021	594235	2660594	0	0	-	-	-	0
Chav-022	594203	2660593	0	2	-	-	-	1
Chav-023	594194	2660579	0	0	-	-	-	0
Chav-024	594286	2660548	0	0	-	-	-	0
Chav-025	594327	2660511	2	1	-	-	-	0
Chav-026	594342	2660514	0	0	-	-	-	0
Chav-027	594718	2660510	3	2	Trend	120	-	0
Chav-028	594732	2660521	2	-	Trend	349	-	0
Chav-029	594816	2660518	2	-	-	-	-	0
Chav-030	594902	2660575	3	3	S/D	333	86	0
CBARS-300	595153	2667992	3	3	S/D	162	82	0
CBARS-300	595153	2667992	3	3	S/D	152	86	0
CBARS-300	595153	2667992	3	3	S/D	1	46	0
CBARS-300	595153	2667992	3	3	S/D	5	5	0

CBARS-300	595153	2667992	3	3	S/D	130	71	0
CBARS-300	595153	2667992	3	3	S/D	130	68	0
CBARS-300	595153	2667992	3	3	S/D	31	78	0
CBARS-301	595139	2667981	0	0	-	-	-	0
CBARS-302	595129	2667967	3	-	-	-	-	0
CBARS-303	595134	2667976	3	2	S/D	53	34	0
CBARS-304	595116	2667962	0	0	Trend	340	-	0
CBARS-305	595107	2667953	3	-	Trend	190	-	0
CBARS-305	595107	2667953	3	-	Trend	336	-	0
CBARS-306	595068	2667950	4	0	Trend	340	-	0
CBARS-307	595033	2667952	0	2	Trend	237	-	0
CBARS-308	595030	2667933	3	3	-	-	-	0
CBARS-309	595025	2667913	1	3	-	-	-	1
CBARS-310	595016	2667909	1	4	Trend	51	-	0
CBARS-311	595006	2667906	1	3	-	-	-	0
CBARS-312	594999	2667901	1	4	-	-	-	0
CBARS-313	594989	2667899	1	3	Trend	60	-	0
CBARS-314	594982	2667899	1	3	Trend	40	-	0
CBARS-314	594982	2667899	1	3	Trend	144	-	0
CBARS-314	594982	2667899	1	1	-	-	-	0
CBARS-315	594973	2667899	1	1	-	-	-	0
CBARS-316	594944	2667871	2	1	Trend	30	-	0
CBARS-317	594753	2667765	0	0	-	-	-	0
CBARS-318	594773	2667761	0	0	-	-	-	0
CBARS-319	594787	2667773	0	0	-	-	-	0
CBARS-320	594861	2667796	0	0	-	-	-	0

CBARS-321	594846	2667819	0	2	Trend	75	-	0
CBARS-321	594846	2667819	0	2	Trend	140	-	0
CBARS-321	594846	2667819	0	2	Trend	160	-	0
CBARS-322	594822	2667827	1	2	Trend	70	-	0
CBARS-322	594822	2667827	1	2	Trend	310	-	0
CBARS-322	594822	2667827	1	2	Trend	160	-	0
CBARS-323	594859	2667821	8	-	-	-	-	0
CBARS-324	594876	2667843	4	0	Trend	336	-	0
CBARS-325	594903	2667800	1	-	-	-	-	0
CBARS-326	594976	2667825	2	-	-	-	-	0
CBARS-327	594985	2667829	4	0	Trend	332	-	0
CBARS-328	594960	2667791	8	-	-	-	-	0
CBARS-329	594950	2667799	0	0	-	-	-	0
CBARS-330	594908	2667844	0	0	-	-	-	0
CBARS-331	594934	2667866	8	-	Trend	18	-	0
CBARS-332	594936	2667866	3	-	Trend	42	-	0
CBARS-332	594936	2667866	3	-	Trend	70	-	0
CBARS-333	594919	2667885	0	1	Trend	70	-	0
CBARS-334	594922	2667893	0	0	-	-	-	0
CBARS-335	594921	2667895	3	1	Trend	240	-	0
CBARS-336	594930	2667908	0	0	S/D	152	70	0
CBARS-337	594952	2667905	2	-	Trend	16	-	0
CBARS-338	595965	2667883	1	-	Trend	52	-	0
CBARS-339	594943	2667836	8	-	-	-	-	0
CBARS-340	594974	2667784	0	0	-	-	-	0
CBARS-341	595015	2667789	4	0	Trend	123	-	0

CBARS-342	595097	2667825	8	-	-	-	-	0
CBARS-343	595053	2667793	0	-	S/D	70	62	0
CBARS-343	595053	2667793	0	-	T/P	70	11	0
CBARS-343	595053	2667793	0	-	Trend	70	16	0
CBARS-343	595053	2667793	0	-	Trend	250	18	0
CBARS-343	595053	2667793	0	-	Trend	70	78	0
CBARS-344	595052	2667789	1	3	S/D	75	78	0
CBARS-345	595035	2667760	4	-	S/D	294	78	0
CBARS-346	594983	2667760	8	-	-	-	-	0
CBARS-347	594999	2668428	1	4	S/D	110	90	1
CBARS-348	594992	2668428	1	-	T/P	242	10	0
CBARS-348	594992	2668428	1	-	S/D	188	64	0
CBARS-348	594992	2668428	1	-	T/P	154	79	0
CBARS-348	594992	2668428	1	-	T/P	134	60	0
CBARS-348	594992	2668428	1	-	Trend	24	-	0
CBARS-348	594992	2668428	1	-	Trend	341	-	0
CBARS-349	595012	2668456	1	2	Trend	333	-	0
CBARS-350	595005	2668469	3	-	Trend	68	-	0
CBARS-350	595005	2668469	3	-	Trend	100	-	0
CBARS-351	595041	2668459	0	-	-	-	-	0
CBARS-352	595079	2668458	0	-	Trend	20	-	0
CBARS-353	595108	2668500	0	-	T/P	210	8	0
CBARS-354	595128	2668468	5	-	Trend	20	-	0
CBARS-355	595133	2668471	1	2	Trend	40	-	0
CBARS-356	595136	2668476	1	-	S/D	52	75	0
CBARS-357	595158	2668494	0	-	S/D	229	86	0

CBARS-357	595158	2668494	0	-	S/D	10	36	0
CBARS-358	595183	2668489	6	-	Trend	345	-	0
CBARS-359	595158	2668397	0	-	T/P	352	2	0
CBARS-359	595158	2668397	0	-	T/P	352	20	0
CBARS-360	595149	2668402	5	-	-	-	-	1
CBARS-361	595198	2668536	0	-	-	-	-	0
CBARS-362	595202	2668575	6	-	T/P	347	15	0
CBARS-363	595189	2668603	0	-	-	-	-	0
CBARS-364	595188	2668603	0	-	-	-	-	0
CBARS-365	595221	2668596	1	2	Trend	50	-	0
CBARS-366	595258	2668595	5	-	-	-	-	0
CBARS-367	595296	2668652	5	-	-	-	-	0
CBARS-368	595304	2668656	1	-	Trend	120	-	0
CBARS-368	595304	2668656	5	-	-	-	-	0
CBARS-369	595320	2668662	5	-	-	-	-	0
CBARS-370	595383	2668678	5	1	T/P	216	27	0
CBARS-371	595365	2668713	1	2	-	-	-	1
CBARS-372	595456	2668718	0	-	-	-	-	0
CBARS-373	595527	2668717	0	-	-	-	-	0
CBARS-374	595576	2668730	0	1	-	-	-	0
CBARS-375	595547	2668844	6	-	Trend	42	-	0
CBARS-376	595541	2668877	6	-	-	-	-	0
CBARS-377	595738	2668877	0	-	S/D	166	70	0
CBARS-377	595738	2668877	0	-	S/D	210	70	0
CBARS-378	595795	2668809	1	-	Trend	0	-	0
CBARS-378	595795	2668809	4	-	-	-	-	0

CBARS-379	595301	2668378	6	-	S/D	121	66	0
CBARS-380	595314	2668323	6	-	S/D	118	64	0
CBARS-380	595314	2668323	5	-	T/P	337	8	0
CBARS-381	595381	2668333	6	-	-	-	-	0
CBARS-382	595400	2668306	6	-	Trend	123	-	0
CBARS-383	595386	2668316	0	2	Trend	74	-	0
CBARS-383	595386	2668316	0	2	Trend	351	-	0
CBARS-383	595386	2668316	0	2	Trend	36	-	0
CBARS-384	595417	2668326	1	2	-	-	-	0
CBARS-385	595416	2668344	6	1	Trend	110	-	0
CBARS-385	595416	2668344	6	1	S/D	290	76	0
CBARS-385	595416	2668344	6	1	S/D	290	86	0
CBARS-386	595454	2668398	0	-	-	-	-	0
CBARS-387	595457	2668428	0	1	S/D	170	70	0
CBARS-388	595502	2668430	0	1	Trend	41	-	0
CBARS-389	595576	2668410	0	-	-	-	-	0
CBARS-390	595607	2668419	6	3	T/P	333	11	0
CBARS-391	595612	2668476	6	3	Trend	40	-	1
CBARS-392	595592	2668528	0	-	-	-	-	0
CBARS-393	595614	2668558	6	-	-	-	-	0
CBARS-393	595614	2668558	1	2	S/D	180	33	0
CBARS-394	595622	2668568	6	-	-	-	-	0
CBARS-394	595622	2668568	1	-	Trend	33	-	0
CBARS-395	595631	2668606	1	-	-	-	-	0
CBARS-396	595632	2668624	1	-	-	-	-	1
CBARS-397	595631	2668646	1	-	-	-	-	0

CBARS-398	595622	2668683	1	-	-	-	-	0
CBARS-399	595598	2668700	3	-	S/D	167	30	0
CBARS-400	595584	2668724	2	-	-	-	-	0
CBARS-401	595585	2668754	2	-	-	-	-	0
CBARS-402	595578	2668803	3	-	-	-	-	0
CBARS-403	595561	2668869	3	-	-	-	-	0
CBARS-404	595578	2668919	2	-	-	-	-	0
CBARS-405	595592	2668924	6	-	Trend	77	-	0
CBARS-406	595591	2668994	2	-	-	-	-	0
CBARS-407	595571	2669015	3	-	-	-	-	0
CBARS-408	595590	2669035	3	-	Trend	356	-	1
CBARS-409	595632	2668361	6	-	Trend	75	-	0
CBARS-410	595635	2668251	2	-	Trend	0	-	0
CBARS-411	595606	2668206	2	-	-	-	-	0
CBARS-412	595569	2668201	0	-	-	-	-	0
CBARS-413	595559	2668200	1	1	Trend	314	-	0
CBARS-414	595526	2668194	1	-	S/D	45	67	0
CBARS-415	595499	2668190	3	2	-	-	-	0
CBARS-416	595461	2668135	4	-	-	-	-	0
CBARS-416	595461	2668135	1	-	-	-	-	0
CBARS-417	595471	2668158	1	-	Trend	82	-	0
CBARS-418	595481	2668167	1	-	-	-	-	0
CBARS-419	595500	2668176	1	-	-	-	-	0
CBARS-420	595547	2668229	2	-	-	-	-	0
CBARS-421	595536	2668245	1	1	-	-	-	0
CBARS-422	595497	2668321	6	-	Trend	250	7	0

CBARS-423	595474	2668347	1	-	S/D	164	45	0
CBARS-423	595474	2668347	1	-	S/D	207	33	0
CBARS-424	595500	2668488	0	-	-	-	-	0
CBARS-425	595488	2668553	1	-	S/D	235	80	0
CBARS-426	595455	2668530	1	-	S/D	236	86	0
CBARS-427	595436	2668513	1	2	S/D	235	83	0
CBARS-428	595392	2668492	4	-	Trend	346	-	0
CBARS-429	595386	2668490	3	-	Trend	248	-	0
CBARS-430	595274	2668432	1	-	Trend	254	-	0
CBARS-431	595158	2668116	0	-	-	-	-	0
CBARS-432	595167	2668089	3	2	-	-	-	0
CBARS-433	595182	2668089	1	-	-	-	-	0
CBARS-434	595187	2668101	1	-	-	-	-	0
CBARS-435	595234	2668100	0	-	-	-	-	0
CBARS-436	595248	2668104	1	3	Trend	47	-	0
CBARS-437	595257	2668108	0	-	-	-	-	0
CBARS-438	595277	2668100	0	-	S/D	180	50	0
CBARS-439	595311	2668115	4	-	Trend	188	-	0
CBARS-439	595311	2668115	2	-	-	-	-	0
CBARS-440	595379	2668110	1	1	Trend	47	-	0
CBARS-440	595379	2668110	2	2	-	-	-	0
CBARS-441	595289	2668182	0	-	-	-	-	0
CBARS-442	595279	2668210	1	2	Trend	40	-	0
CBARS-443	595227	2668209	0	-	-	-	-	0
CBARS-444	595219	2668221	6	-	S/D	252	66	0
CBARS-445	595175	2668225	2	-	Trend	164	-	0

CBARS-446	595147	2668205	2	-	Trend	150	-	0
CBARS-447	595750	2669071	0	-	-	-	-	0
CBARS-448	595711	2669043	2	1	Trend	338	-	0
CBARS-449	595741	2668934	0	-	-	-	-	0
CBARS-450	595817	2668764	1	2	Trend	120	-	0
CBARS-451	595944	2668568	0	-	-	-	-	0
CBARS-452	595940	2668530	1	-	-	-	-	0
CBARS-453	595911	2668439	0	-	-	-	-	0
CBARS-454	595949	2668493	1	-	S/D	67	61	0
CBARS-455	595975	2668519	1	-	S/D	52	70	0
CBARS-456	596082	2668580	2	-	Trend	150	-	0
CBARS-457	596134	2668521	0	-	-	-	-	0
CBARS-458	596160	2668494	1	-	Trend	60	-	0
CBARS-459	596216	2668515	1	-	-	-	-	0
CBARS-460	596156	2668476	1	2	S/D	50	50	0
CBARS-461	596119	2668443	1	3	Trend	65	-	1
CBARS-462	596069	2668416	1	-	-	-	-	0
CBARS-463	596047	2668327	6	-	S/D	88	60	1
CBARS-463	596047	2668327	1	-	-	-	-	0
CBARS-464	596035	2668313	4	-	S/D	48	23	0
CBARS-465	595880	2668342	0	1	-	-	-	0
CBARS-466	595783	2668322	6	-	-	-	-	0
CBARS-466	595783	2668322	1	-	-	-	-	0
CBARS-467	595741	2668386	6	-	-	-	-	0
TRIN-001	594657	2660780	2	3	-	-	-	0
TRIN-002	594868	2660830	2	3	S/D	120	70	0

TRIN-002	594868	2660830	2	3	S/D	120	85	0
TRIN-003	594988	2660544	2	1	-	-	-	0
TRIN-004	594911	2660572	2	2	Trend	344	-	0
TRIN-005	594891	2660599	2	2	Trend	344	-	0
TRIN-006	594886	2660642	2	-	Trend	15	-	0
TRIN-007	594853	2660603	2	-	Trend	340	-	0
TRIN-008	594884	2660528	2	-	-	-	-	0
TRIN-009	594869	2660481	2	1	-	-	-	0
TRIN-010	594799	2660480	2	-	Trend	16	-	1
TRIN-011	594786	2660506	2	-	-	-	-	0
TRIN-012	594820	2660241	0	1	-	-	-	0
TRIN-013	594797	2660244	2	-	Trend	46	-	0
TRIN-014	594783	2660200	0	-	-	-	-	0
TRIN-015	594802	2660146	0	-	Trend	60	-	0
TRIN-015	594802	2660146	0	-	Trend	330	-	0
TRIN-015	594802	2660146	2	-	Trend	357	-	0
TRIN-015	594802	2660146	2	-	Trend	8	-	0
TRIN-016	594813	2660122	2	-	Trend	5	-	0
TRIN-017	594845	2660118	0	-	S/D	56	42	0
TRIN-017	594845	2660118	0	-	S/D	194	15	0
TRIN-018	594846	2660049	0	-	-	-	-	0
TRIN-019	594845	2660011	6	2	-	-	-	0
TRIN-020	594813	2659965	8	-	S/D	48	72	0
TRIN-021	594777	2659968	0	1	-	-	-	0
TRIN-022	594761	2659958	2	1	Trend	10	-	0
TRIN-023	594752	2659922	6	2	S/D	60	74	0

TRIN-024	594788	2659916	6	-	Trend	30	-	1

APPENDIX B

ASSAY RESULTS

Sample ID	Easting	Northing	Au	Ag	Cu (PPM)	Pb (PPM)	Zn (PPM)
BCARS-004	596021	2669588	Low	None-Low	22	67	56
BCARS-014	595987	2669468	Low	Low	22	162	113
BCARS-020	596040	2669718	None-Low	None-Low	1	7	31
BCARS-029	595221	2669364	None-Low	None-Low	2	10	45
BCARS-033	594965	2669086	None-Low	None-Low	13	44	52
BCARS-067	595307	2669231	None-Low	None-Low	10	19	26
BCARS-078	595408	2668323	None-Low	None-Low	1	3	32
BCARS-093	596045	2669415	None-Low	None-Low	1	15	61
BCARS-097	595947	2669322	None-Low	Moderate	58	4410	26
BCARS-107	594842	2668078	Low	Moderate	38	474	131
BCARS-109	594904	2668106	None-Low	None-Low	14	13	30
BCARS-116	594773	2668020	Low	High	105	1070	185
BCARS-119	594717	2667965	Low	Very High	315	3620	223
BCARS-121	594704	2667950	Low	Very High	164	1610	350
BCARS-151	594608	2668022	Low	None-Low	27	94	123
BCARS-182	594822	2668369	None-Low	None-Low	12	36	44
BCARS-190	594997	2668409	None-Low	Moderate	319	1060	5500
BCARS-206	595893	2668484	None-Low	None-Low	2	17	31
BCARS-216	595946	2669094	None-Low	None-Low	2	29	28
BCARS-309	595025	2667913	None-Low	High	189	1265	127
BCARS-347	594999	2668428	None-Low	None-Low	3	28	37
BCARS-371	595365	2668713	Low	Moderate	36	398	64
BCARS-391	595612	2668476	None-Low	None-Low	1	18	29
BCARS-408	595590	2669035	None-Low	None-Low	1	13	27
BCARS-461	596119	2668443	None-Low	None-Low	2	16	32
BCARS-463	596047	2668327	None-Low	None-Low	1	17	31
CHAV-001	594856	2660230	Low	Low	7	23	28
CHAV-022	594203	2660593	None-Low	None-Low	3	14	30
TRIN-024	594788	2659916	None-Low	None-Low	<1	14	53